Heliyon 9 (2023) e12685

Contents lists available at ScienceDirect

Heliyon

journal homepage: www.cell.com/heliyon

Review article

Synthesis and applications of graphitic carbon nitride (g-C_3N_4) based membranes for wastewater treatment: A critical review

Muhammad Azam Qamar [a,*], Mohsin Javed [a], Sammia Shahid [a], Mohammad Shariq [b], Mohammed M. Fadhali [b,e], Syed Kashif Ali [c], Mohd. Shakir Khan [d]

[a] Department of Chemistry, School of Science, University of Management and Technology, Lahore, 54770, Pakistan
[b] Department of Physics, College of Science, Jazan University, Jazan, 45142, Saudi Arabia
[c] Department of Chemistry, College of Science, Jazan University, Jazan, 45142, Saudi Arabia
[d] Department of Physics, College of Science, Al- Zulfi, Majmaah University, Al- Majmaah, 11952, Saudi Arabia
[e] Department of Physics, Faculty of Science, Ibb University, Ibb, 70270, Yemen

ARTICLE INFO

Keywords:
g-C_3N_4
Antifouling
Water purification
Separation membrane
Photodegradation
Nanofiltration

ABSTRACT

Semiconducting membrane combined with nanomaterials is an auspicious combination that may successfully eliminate diverse waste products from water while consuming little energy and reducing pollution. Creating an inexpensive, steady, flexible, and diversified business material for membrane production is a critical challenge in membrane technology development. Because of its unusual structure and high catalytic activity, graphitic carbon nitride (g-C3N4) has come out as a viable material for membranes. Furthermore, their great durability, high permanency under challenging environments, and long-term use without decrease in flux are significant advantages. The advanced material techniques used to manage the molecular assembly of g-C3N4 for separation membrane were detailed in this review work. The progress in using g-C3N4-based membranes for water treatment has been detailed in this presentation. The review delivers an updated description of g-C3N4 based membranes and their separation functions and new ideas for future enhancements/adjustments to address their weaknesses in real-world situations. Finally, the ongoing problems and promising future research directions for g-C3N4-based membranes are discussed.

1. Introduction

Concerns over the safety of the world's water supply have become more important over the last several decades. Traditional water filtration technologies may solve many issues related to poor water quality, but their effectiveness, expense, or occupied area restrict them in most situations [1,2]. Most impurities may be eliminated from wastewater using membrane separation as a new technique by physically sieving using pressure, concentration, or an electrical gradient as a driving force. It has been a propitious and dependable technology for water treatment because of its easy operation, environmental friendliness, and energy economy [2,3]. New micropollutants, such as pesticides, endocrine disruptors, medicines, and other human-produced micropollutants, are entering the aquatic environment and posing new technical hurdles to membrane separation [4,5]. To address the shortcomings of traditional membrane

* Corresponding author.
E-mail address: qamariub@gmail.com (M.A. Qamar).

https://doi.org/10.1016/j.heliyon.2022.e12685
Received 19 August 2022; Received in revised form 21 October 2022; Accepted 21 December 2022
Available online 3 January 2023

technologies, novel materials such as carbon nanotubes (CNTs), carbon quantum dots (CQD), graphene, and g-C_3N_4 nanosheets (GCNS) were used to develop membranes [6–8]. Because of its porous properties, electrical, electronic structures, and physicochemical stability, g-C_3N_4 has received a lot of interest. g-C_3N_4 provides several benefits over conventional carbon-based materials, including superior optical qualities, a unique electronic structure, adaptability, and low environmental impact [9,10]. The g-C_3N_4 framework's shape and surface chemistry may be tweaked by incorporating several delicate functionalities to manage further its solubility, photoelectric characteristics, and compatibility with diverse surfaces. g-C_3N_4 has been described as metal free photocatalyst and over 9500 publications have been published on its synthesis, basic features, and potential use [11]. g-C_3N_4 is now attracting attention in different domains like sensing, photocatalysis, energy conversion, and separation [12,13]. Because of its efficient light-absorption and low bandgap, g-C_3N_4 is predominantly employed for photocatalytic water breakdown, CO_2 reduction, and degradation of toxins [14–16]. The photoluminescence (PL) capabilities of g-C_3N_4 enable it to be applied as turn-on biochemical and biosensor for detecting Cu^{2+}, Ag^{+}, Fe^{3+}, Hg^{2+}, and Cr^{2+} ions. g-C_3N_4 has also been used effectively in biological studies because of its biocompatibility [17,18]. Yang's group, for example, found that a g-C_3N_4/up-conversion nanoparticle composite effectively prevents tumor growth by creating reactive oxygen species in response to NIR laser excitation [19–22].

The introduction of GCNS into membrane separation applications breathes new life into developing highly effective separation membranes. This nanomaterial exhibits customizable surface properties, high porosity, and stiff and permanent pore structures, making it superior to typical absorbent materials like zeolites in terms of functionality [23]. According to molecular dynamics simulations, GCNS with a nanopore diameter of 1.48 nm may effectively block the majority of ions (at least 70%). At the same time, the water permeability can approach 91.0 $L\,m^{-2}\,h^{-1}\,bar^{-1}$ [14].

Apart from its unique energy band, g-C_3N_4 also has several other advantageous properties such as processability, high chemical stability, & non-toxic origin [24]. As a result, it has great prospective in membrane filtration applications, particularly for visible-light-driven photocatalytic activity [25]. Instigated by the aforementioned benefits, g-C_3N_4 based advanced membranes can demonstrate greater efficiency than usual membranes in terms of separation and self-cleaning [26]. Thus, the newly produced g-C_3N_4 based hybrid membranes can accomplish the desired removal efficiency for a wide range of pollutants as well as outstanding membrane fouling resistance. Besides, the reduced energy consumption to retrieve permeate, makes it possible to apply membrane filtration to treat wastewater on a large scale and for an extended period. Fig. 1 explains the general applications of g–C_3N_4–based membrane mainly discussed in the current review.

As a result, g–C_3N_4–based membrane separation has emerged as one of the most critical applications of g-C_3N_4. So far, there have been a lot of reviews primarily aiming at g-C_3N_4 syntheses, modifications, characteristics, and catalytic uses. To our knowledge, however, no comprehensive analysis of g–C_3N_4–based membranes has been reported. The study aims to review (1) current advances in production, (2) diversity and depth in applications, as well as (3) upcoming challenges and prospects for g–C_3N_4–based membrane technology.

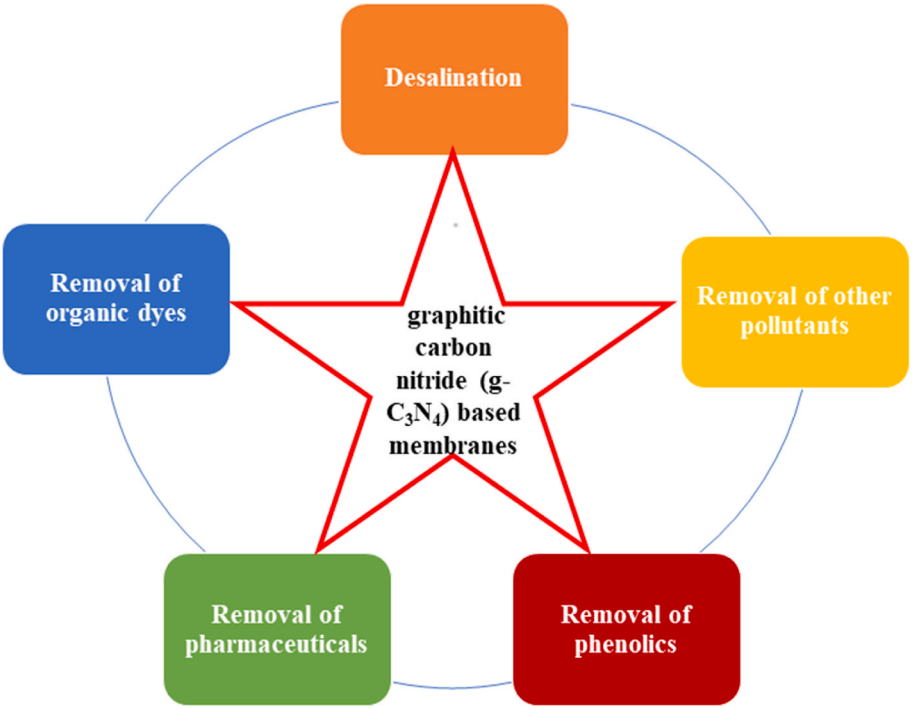

Fig. 1. General application of g-C_3N_4 based membranes in diverse fields.

1.1. Fabrication and structural characteristics of g-C_3N_4 based membranes

.

1.2. Assembly and properties of g-C_3N_4

Carbon nitride (C_3N_4) has been studied since 1834, but its potential application was not fully realized till Wang et al. applied it for water splitting [11,27]. Under normal conditions the g-C_3N_4 is the most established allotrope of the C_3N_4 due to its distinctive physicochemical qualities. In general, g-C_3N_4 is made up of the tri-*s*-triazine and heptazine units joined by planar amino groups, with van der Waals forces acting on the interlayers [28]. To compose g-C_3N_4, two basic tectonic units are essential: triazine (C_3N_3) and tri-*s*-triazine (C_6N_7). Its whole structure is composed of ring planes conjugated to each other (Fig. 2 (a, b) [21,28]. A graphite-like lattice structure is present in the layered material, associated with van der Waals interactions. During the formation of the layers, nitrogen and carbon atoms alternated in a hexagonal pattern. The potential total surface area of g-C_3N_4 may go as high as 2500 $m^2 g^{-1}$ [26,29].

Both types of units may be produced using the condensation process with appropriate precursors. According to the experimental findings and theoretical calculations, it is observed that the C_6N_7 subunits are much durable than the C_3N_3 units. Ideally g-C_3N_4 should have C═N bonds without π-electron localization in the ground state [30,31]. Although g-C_3N_4 typically has tiny hydrogen on the terminal edges, this may be due to defects on the surface. Because of the presence of hydrogen and surface imperfections, g-C_3N_4 exhibits distinct surface features that are critical for a wide range of photocatalytic applications. The surface modification of g-C_3N_4 may be modified at the molecular level by molecular modification and surface engineering, ensuring that the structure retains sufficient flexibility [25]. Owing to C_6N_7 ring system, g-C_3N_4 exhibits exceptional thermal stability across a wide range of temperatures. Thermogravimetric analysis (TGA) exhibits that g-C_3N_4 has ability to tolerate high temperatures even in the presence of pure oxygen. The thermal breakdown of g-C_3N_4 begins at 630 °C and is completed at 750 °C. g-C_3N_4 undergoes natural breakdown, rather than being oxidized by oxygen, which is thought to cause weight loss. In addition, g-C_3N_4 has excellent chemical stability in various solvents (e.g., alcohol, water etc.). Because of its remarkable solvent resistance, g-C_3N_4 is an extraordinary substance for fluid reactions.

With the help of GCNS that have been exfoliated from their bulky equivalents, the g-C_3N_4 membrane may be created on different substrates using a variety of assembly procedures [32]. So, the acquired free-standing g-C_3N_4 film/membrane exhibits the same physiochemical properties as those of the nanosheet building block. Changing the building components of the nanosheet makes it possible to provide unique features to the resulting g-C_3N_4 film/membrane. The lone-pairs of electron (sp^2) present on the nitrogen of g-C_3N_4 can be used to modify the distance between layers in the membrane [24]. The distance between layers of the formed membrane might be increased by 10.8 Å by intercalating sulphate anions into the protonated g-C_3N_4 nanostructure using traditional filtration process.

It is important to note that g-C_3N_4 exhibits good photocatalytic activity when exposed to visible light. Its conduction band (CB) location is at 1.1 eV, while its valence band (VB) position is at +1.6 eV [25]. g-C_3N_4 is yellow due to optical absorbance at 460 nm and may take advantage of utilization of visible-light irradiation from the sun [33]. Thermal condensation or Sulphur doping may be used to modify the bandgap, and this is related to the production of defects, nanostructures, and orientations. But, g-C_3N_4 has the drawback of having comparatively poor visible-light sensitivity because of fast electron-hole pairs recombination [20,34].

Under appropriate light radiations on g-C_3N_4, the electron-hole pairs are induced that might be used to explain its photocatalytic activity. The production of reactive oxygen species can be explained well via Eqs. (1)–(5) [35]. The excited electrons in g-C_3N_4 will travel from VB to CB and produce superoxide anion radicals ($\dot{O}_2^-$) and hydroxyl radicals. These photogenerated holes (h^+), $\dot{O}_2^-$, and

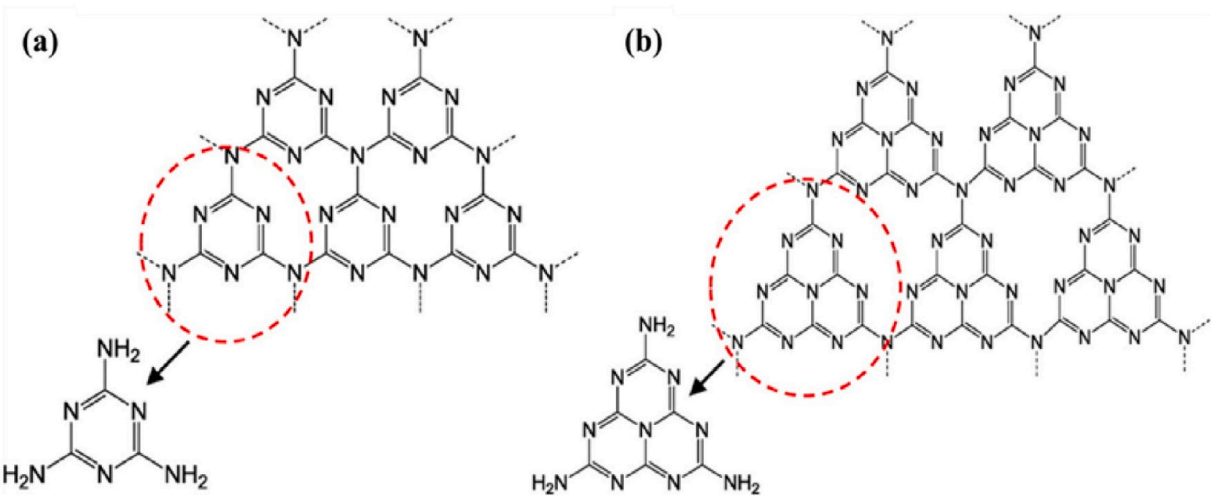

Fig. 2. Structure of Triazine (a) [21] and tri-*s*-triazine (b) in g-C_3N_4 [28].

hydroxyl radicals act as oxidizers for organic contaminants [25].

$$g - C_3N_4 + hv \rightarrow g - C_3N_4(e^-/h^+) \quad (1)$$

$$g - C_3N_4\ (e) + O_2 \rightarrow \dot{O}_2 \quad (2)$$

$$g - C_3N_4(e) + H_2O/OH^- \rightarrow \dot{O}H \quad (3)$$

$$\dot{O}H/\dot{O}_2^- + Pollutant \rightarrow Degraded\ Products \quad (4)$$

$$h^+ + Pollutant \rightarrow Degraded\ Products \quad (5)$$

1.3. Synthesis of g-C_3N_4 based membranes

Polymeric g-C_3N_4 is most commonly used to fabric next-generation membranes due to its distinctive graphite-like laminar structure, amenably changeable pore size and structure, and ability to be easily altered in terms of functionality. So far, several methodologies have been established to structure g–C_3N_4–based membranes with high permeability and biocompatibility. Currently, g-C_3N_4 is not only being used to construct a self-supporting membrane, but also can be integrated with supporting substrates to form a lamellar membrane, or implanted as nanofillers in an organic polymer matrix to form a hybrid membrane. Several approaches have been devised so far to manufacture g–C_3N_4–based membranes with high specificity and permeability. g–C_3N_4–hybridised membranes show better mechanical and swelling expansion resistance as compared to g-C_3N_4 multilayered membranes produced by vacuum filtration. The better properties of g–C_3N_4–hybridised membranes were endorsed to the excellent interface between g-C_3N_4 and the bulk of organic polymers [21]. The techniques that are utilized for membrane manufacture may be summarized below.

1.3.1. Blending

Blending is a design technique for g–C_3N_4–based membranes, and it is particularly relevant for g–C_3N_4–based mixed matrix membranes (MMMs), which are currently under development. The simplicity of operation and the ease of application scale up are two most notable benefits of this technology. More importantly, compared to lamellar membranes that include just the naked g-C_3N_4 layer, g-C_3N_4 surrounded by polymers is likely to be significantly more stable, resulting in the enduring strength of such g–C_3N_4–based membranes. Substrate-based blending and substrate-free blending are the two important approaches which have been devised to construct g–C_3N_4–based MMMs. g–C_3N_4–based MMMs are often prepared via substrate-based mixing, particularly for pervaporation. The strength and stability of the hybrid membranes may be improved by using porous membranes like PAN and PES as support. Three steps are normally included in the application of these techniques: (a) combining with polymeric dopes to generate a casting liquid; (b) applying the spin-coating process for casting the solutions onto the porous layer to form a thin film; (c) drying or cure treatment to

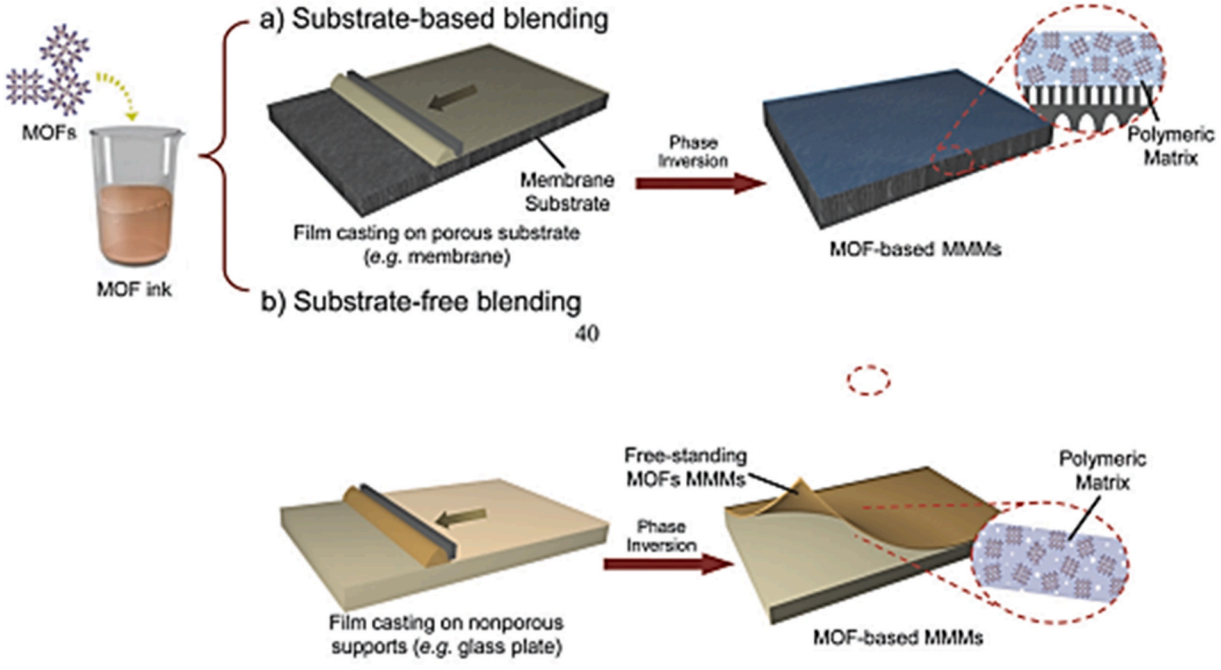

Fig. 3. Synthesis of g–C_3N_4–based mixed matrix membranes by substrate-based blending method (a) substrate free blending method (b) [36].

remove the solution. A g–C_3N_4–based MMMs may be produced on the surface of the membrane supports after these operations (Fig. 3 (a, b) [36]. It should be noted that the structure and characteristics of as obtained MMMs are often affected by the g-C_3N_4/polymer mixing ratio. By adding g-C_3N_4 nanofibers into a hydrophobic polymer sodium alginate (SA) matrix, the MMMs with good water separation and penetration capacities for water/ethanol mixtures were obtained [25]. Intermolecular hydrogen bonding existing between –OH and –COOH group of SA and the $–NH_2$ and –NH groups of g-C_3N_4 are weak the in the composite membrane. As the concentration of GCNS in the membrane rises, cross-sectional images of the SA/g-C_3N_4 hybrid membrane enhance well-aligned amorphous morphology. However, if the concentration of g-C_3N_4 is too high, the nanosheets alignments become disordered [37]. The solution-blending and spraying approach was employed by Wang et al. to create CPVA-g-C_3N_4 gas permeation membrane on PAN and PES ultrafiltration membranes by using 2D g-C_3N_4 nanofibers as fillers, PVA as polymer matrices, and succinic acid as cross-linker [38]. g-C_3N_4, succinic acid and the PVA matrix formed an interfacial bond that resulted in strong swelling resilience and mechanical stability in the membrane with thickness of about 50 μm. Wang et al. coupled polydopamine-modified g-C_3N_4 (PDA@O-g-C_3N_4) nanostructures with PVA polymer to create new hybrid pervaporation membranes that improved compliance of g-C_3N_4 with polymer matrix [39] (Fig. 4).

Due to the fact that water purification process in substrate-free blending is not constrained by the type of material of the support, this type is more versatile in fabricating the g–C_3N_4–based MMMs. In substrate-free blending, the casting solutions are cast onto non-porous supports such as glass pieces to assure that the membrane peeled away following the phase change. In another study, the casting solution sulfonated poly (ether ether ketone) (SPEEK) was mixed with g-C_3N_4 and the corresponding mixture was casted on glass plates. Then g-C_3N_4/SPEEK nanocomosite free-standing membrane was yielded by peeled off after sequential vacuum drying and cooling [40]. In blending technique, the phase conversion can be induced with or without solvent [41]. For instance, Wang et al. employed non-solvent phase conversion to produce PES-CN/rGO membrane using rGO and GCNS [42]. In this process, the CN/rGO was mixed PES in mixed solvent to get casting solution. The resultant solution was casted on glass pane, evaporated for 20 s and then phase inversion was induced by dipping the formed membrane in deionized water. It is possible to boost the exchange rate between solvent and non-solvent by using precise quantity of CN/rGO. When reaction polymers are mixed with blending fillers via the conventional mode, then phase transition will definitely result in unequal distribution of nanofillers and membrane channel obstruction [43]. Li et al. solved this issue by developing a unique magnetically induced freeze casting process to facilitate the development of g–C_3N_4–based MMMs. The membrane fabrication method is detailed in Fig. 5, where magnetic Fe_2O_3 particles in situ were adhered on the surface of g-C_3N_4 and thus used to promote the g-C_3N_4 movement to the membrane surface under magnetic field. Hence a combined phase inversion and directional freeze casting process was employed to develop Fe_2O_3/g-C_3N_4/PVDF membranes (FCMs). Light absorption performance and interfacial affinity of g-C_3N_4 pollutant rejection were greatly facilitated by ordered latticed macroporous structure of FCMs [44].

Ultimately, the blending approach is a successful and simple way of manufacturing g–C_3N_4–based MMMs, owing to its simplicity, high repeatability, and ease of scaling-up. g-C_3N_4 and g g–C_3N_4–based composites may be readily incorporated into a polymer matrix

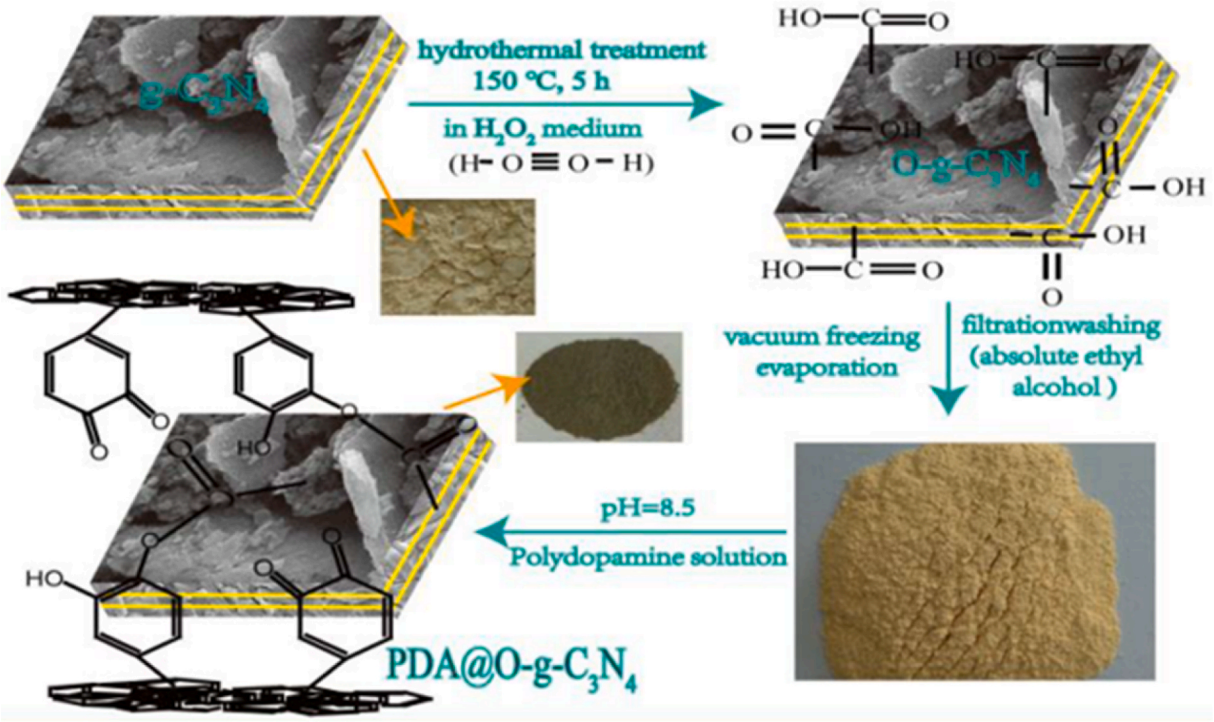

Fig. 4. Illustration of substrate-based blending for the synthesis of g–C_3N_4–based MMMs [39].

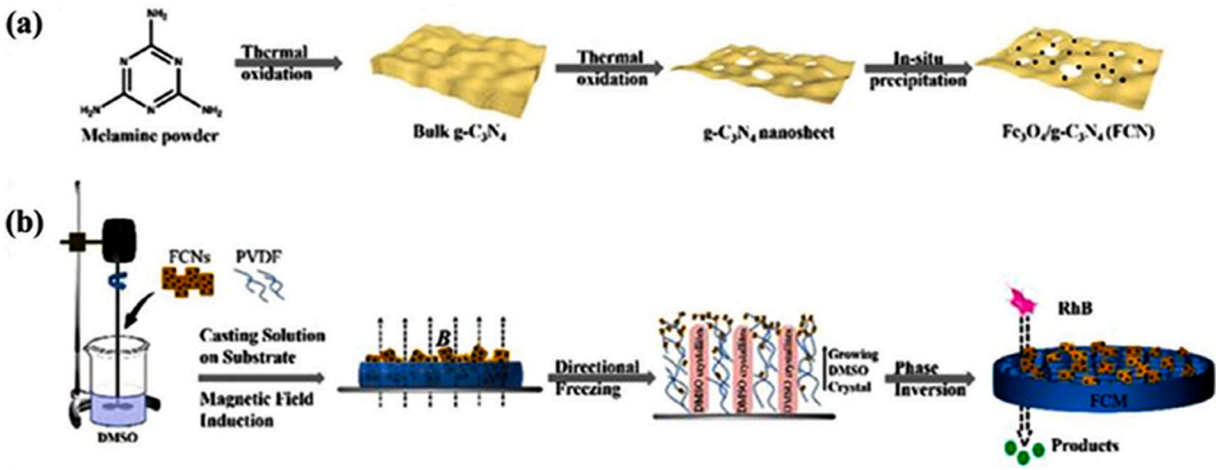

Fig. 5. Schematic illustration of synthesis of (a) FCNs and (b) FCMs by substrate-free blending [44].

via mixing with polymers casting solution, phase inversion, and solution casting, allowing the production and remolding of polymer membranes to ensue concurrently. It should be noticed that g-C_3N_4 embedded hybrid membranes may emit g-C_3N_4 particles, reducing their performance and harming the environment. As a result, future blending procedures should limit or prevent the leaking of g-C_3N_4 components from polymeric membranes.

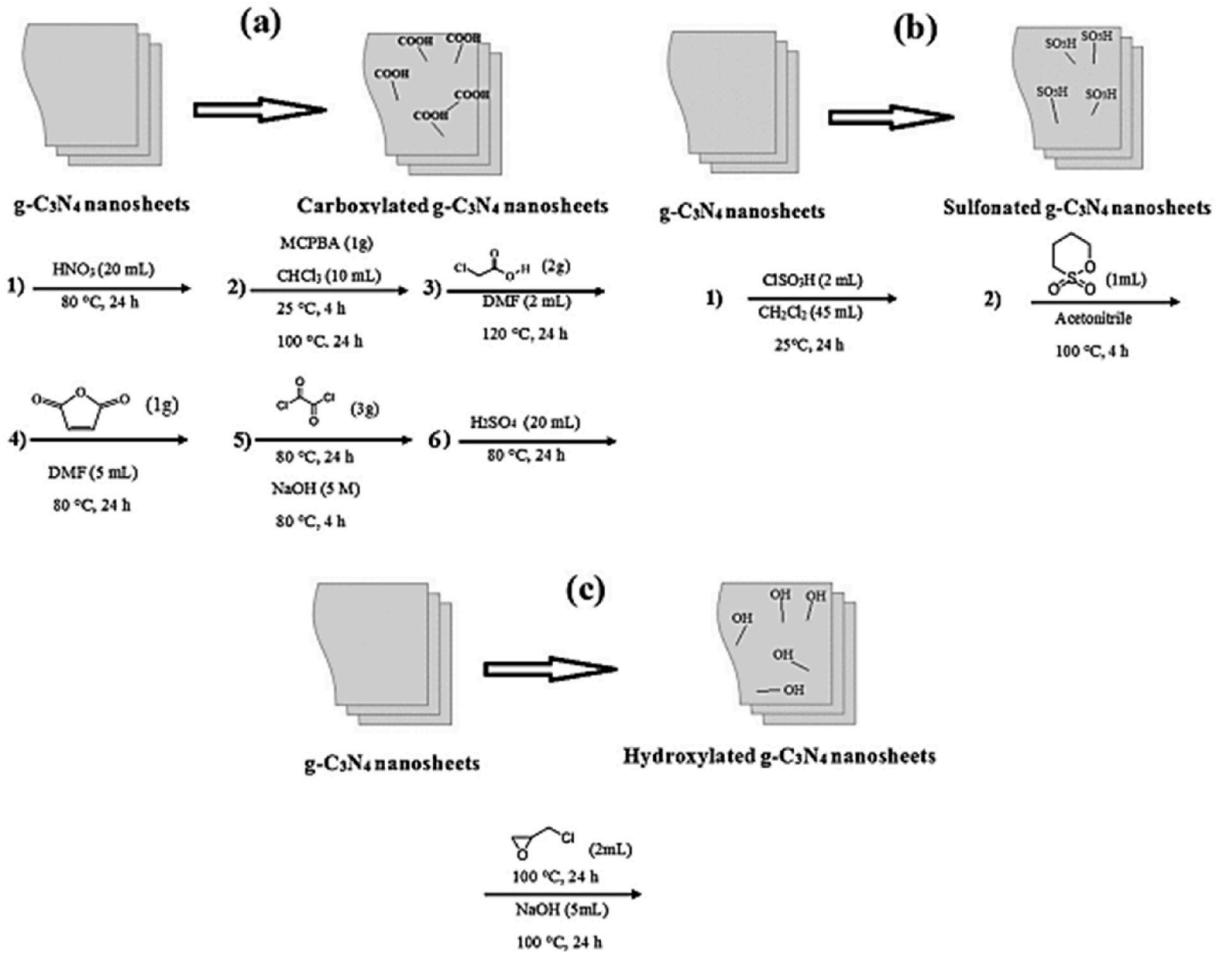

Fig. 6. The schematic diagram for functionalization of g-C_3N_4 by (a) –COOH, (b) –SO_3H and (c) –OH [46].

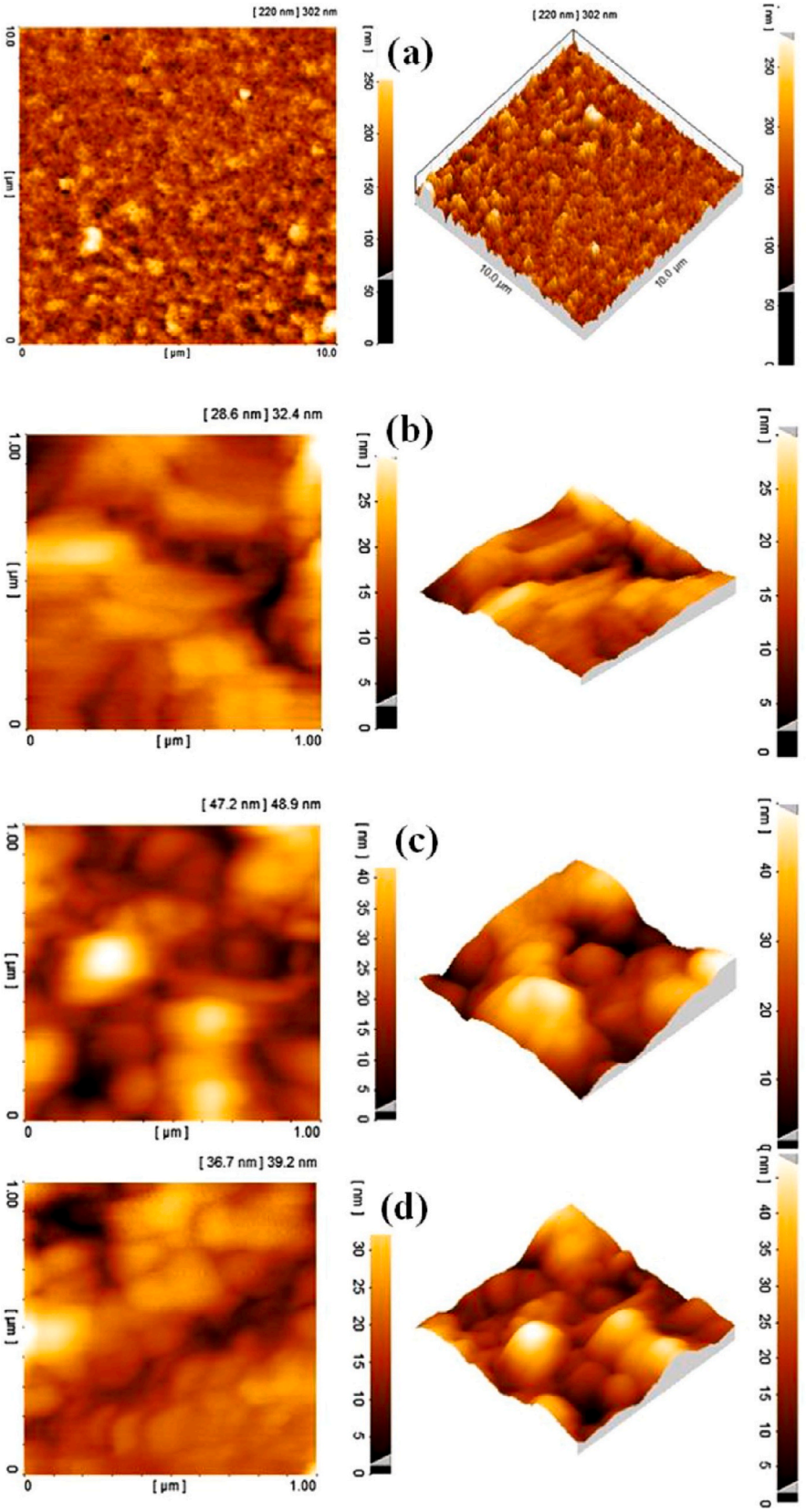

(caption on next page)

Fig. 7. Two and three-dimensional AFM images of TNF membranes imbed with(a) unmodified g-C_3N_4 (b) g–C_3N_4–COOH (c) g–C_3N_4–SO_3H and (d) g–C_3N_4–OH functionalized nanosheets [46].

1.3.2. Interfacial polymerization

A typical way of producing a skinny activated polyamide layer is the reaction of two monomers on the interface of a polymer substrate, which is known as the interfacial polymerization process (IP). It is a successful technique of fabricating high-performance thin film nanocomposites (TFN) membranes by incorporating extremely hydrophilic g-C_3N_4 into the PA layer of a TFC. The characteristics of the PA layer (morphology, tortuosity, and thickness) are significantly improved after the integration of g-C_3N_4 into the PA layer, because of the nanoscale diameter and pore structure of g-C_3N_4. Furthermore, the incorporated g-C_3N_4 may offer additional channels for transport without sacrificing selectivity in the hybrid membrane. Gao et al. for example, distributed acidified g-C_3N_4 nanosheets into an aqueous solution of *m*-phenylenediamine (MPD), which was then utilized to create an integrated PA layer by polymerizing MPD and trimesoyl chloride (TMC) via IP. A TFN membrane entrenched with aCN group demonstrated good antifouling properties and water permeableness. In contrast, the inconsistency between the polymers and the nanoparticles causes the aggregation of g-C_3N_4 in the PA layer. During interfacial polymerization, this process would obstruct the reaction between monomers, resulting in the formation of a faulty PA layer and, ultimately, a reduction in the efficiency of TFN membranes. Piperazine (PIP) and TMC were utilized to make TFN membranes via IP, which promoted the dispersion of GCNS in the PA layer and strengthened the interfacial contacts [45]. The dispersion of GCNS in the PA active layer was enhanced by modifying GCNS with diverse functional groups, such as –COOH, –SO_3H, and –OH as shown in Fig. 6 (a-c) [46]. The membranes containing GCNS functionalized with –COOH displayed the best water permeability and salt rejections performance among the group. The atomic force microscopy and contract angle measurements demonstrated that the designed GCNS could considerably decrease the surface roughness of membranes while increasing the hydrophilicity, thereby improving the permeation of the membranes as shown in Fig. 7a-d [46].

The introduction/functionalization of g-C_3N_4 into the active PA layer via the IP process has been generally regarded as a viable method of boosting the effectiveness of TFC membranes. When g-C_3N_4 nanoarchitectures were combined with TFC membranes, then the resultant membranes typically showed significantly higher permeance and salt rejection than original membranes. The production of TFN membranes is hindered by the weak interactions between g-C_3N_4 and the PA layer and the ease with which g-C_3N_4 nanoparticles are aggregated in the PA layer. Future studies should focus on modifying g-C_3N_4 particle size and shape, optimizing their distribution within polymer matrixes, and enhancing TFN membrane structural strength.

1.3.3. Alternative synthesis methods for g-C3N4-based membranes

Membrane performance is intimately tied to the evolution of fabrication methods, which may considerably impact the physicochemical parameters of g-C3N4-based membranes. As an alternative to the relatively mature membrane production methodologies outlined above, various developing membrane processing parameters have also been used to create g-C3N4-based membranes. Zhang et al. for example, used a potentio-static anodization approach to combine g-C3N4 quantum dots with TiO_2 nanotube array (TNA) to produce g-C3N4/TNA membranes that exhibited improved antifouling performance, photocatalytic activity and permeate flux when tested with water that contains *Escherichia coli* [47]. These improved properties of g-C3N4/TNA membranes were attributed to their high porosity of 72%, straight channels, and self-ordered patterns (Fig. 8) [47].

An electrospinning process is a traditional approach for fabricating nanofibers from a viscid polymeric solution, and it has been effectively used to design g-C3N4-integrated nanofibrous membranes. For example, a unique g-C3N4 nanofiber-coated Al_2O_3 hollow fiber membrane (NF-nsGCN/Al_2O_3) has been developed by electrospinning method. The membrane was formed by coating the top of an Al_2O_3 hollow fiber membrane with a g-C3N4 nanosheet-embedded PAN nanofiber and then subjecting it to thermal treatment to harden [48]. High permeation and rejection, as well as fouling resistance and self-cleaning performance were achieved for the NF-nsGCN/Al_2O_3 membranes through the use of distinctive characteristics such even nanofiber morphology, sparse lattice and good water affinity. This membrane was used in oilfield water treatment.

Apart from being a cost-effective way of bettering the functioning of the existing membranes, surface modification may also be used

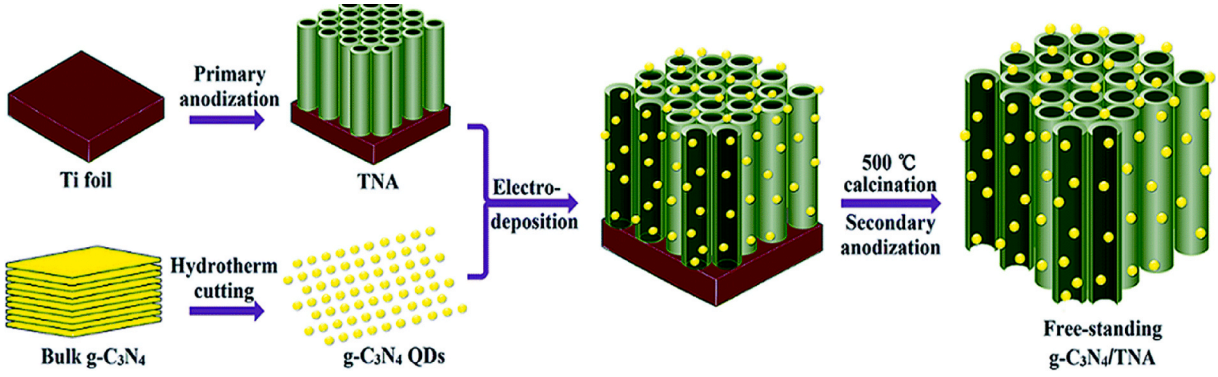

Fig. 8. Schematic of the 3D g-C3N4/TNA preparation [47].

to create new membranes. This method involves the application of a g–C_3N_4–based layer to the membrane surface either by coating it or by grafting [49]. For designing g–C_3N_4–based hybrid membranes, several surface modification methods have been used, including self-assembly (using UV/plasma/chemical agents), vacuum filtration (using chemical agents), dip coating (using cross-linking), interfacial polymerization (using electrospinning), and grafting (using chemical agents) [50–52]. The most widely utilized technique is vacuum filtration because it is a quick way to make consistent g–C_3N_4–based composites on substrate materials. In this technique thickness of the laminate can be modified by changing the amount of g-C_3N_4. However, the mechanical strength and chemical stability of the resulting membrane may be insufficient. As a result, various additional modification techniques are combined to produce highly interactive g–C_3N_4–based composite material, such as self-assembly and the graft polymerization, etc. [10]. Such as Liu et al. modified TiO_2/g-C_3N_4 by intercalating into GO nanosheets via vacuum assisted self-assembly technique as shown in Fig. 9 [53]. The developed GO/g-C_3N_4 @TiO_2 nanosheet exhibited 40 times high permeation flux than GO sheets [53].

Matrix modification is performed in fabrication of g–C_3N_4–based membranes. Using this method, g–C_3N_4–based compounds could be inserted to fill the spaces between membrane substrates in the form of nanofillers [21]. The existing synergistic impact between additives and matrix can alter both the inner and surface of the membrane. Since the surface modification has the drawback liberating g–C_3N_4–based components from the modified membrane surface, it is a competitor modifying technique [54]. So, macro void interruptions occur due to the instability of g–C_3N_4–based nanomaterials with their surrounding matrix. Furthermore, most of g–C_3N_4–based nanomaterials are suppressed inside the framework and unable to captivate light; thus, they compromise their photocatalytic efficacy.

The in-situ thermal condensation method for the synthesis of g–C_3N_4–based membrane is also a good technique. It involves the mixing of substrates with the precursor or immersed into the precursor. The direct development of g-C_3N_4 on membranes resulted from the subsequent calcination at a high temperature. Since the membrane's temperature stability is obviously important, this method is essentially only applicable to inorganic membranes. The remarkable mechanical stability or flexibility of the inorganic substrates can be preserved in g–C_3N_4–based membranes generated by thermal condensation, in addition to the growing photocatalytic activity. For example, Shen et al. developed filter-membrane shaped CF/C_3N_4 fabric by calcining a mixture of carbon fibre (CF) cloth and a saturated urea solution at 550 °C for 3 h [55]. Carbon paper made from cellulose was laid above a layer of urea, and then g-C_3N_4 nanosheets were produced using chemical vapor deposition and plasma treatment on the CCP surface by Dou et al. [56]. Strong interaction between g-C_3N_4 and the substrate can be achieved during high-temperature sintering, which is beneficial for the secure fixing of photocatalyst coating. Increasing the amount of photoactive component in the composite membranes through several coating methods resulted in better photodegradation performance [57].

Wu et al. constructed composite membranes for nanofiltration by the filtration-assisted assembly of graphene oxide and graphitic carbon nitride nanosheets employing glycine as a molecular linker. Interestingly, experimental and characterization results demonstrated that glycine and g-C_3N_4 could increase the interlayer spacing of pure GO membranes, but the former did so at the expense of smaller nanochannels, and the latter resulted in larger ones. With hyperbranched polyethyleneimine (HPEI) coating, a 116-nm-thick Gly-GO/g-C_3N_4 membrane showed good separation performance for organic dye solutions (feed concentration, pH, etc.). Long-term stability studies showed this membrane's 90%–93% dye rejection and minor permeance reduction over 40 h, indicating satisfactory stability [58]. CdS/g-C_3N_4/rGO nanocomposites were produced via immersion precipitation and phase inversion. The photocatalyst

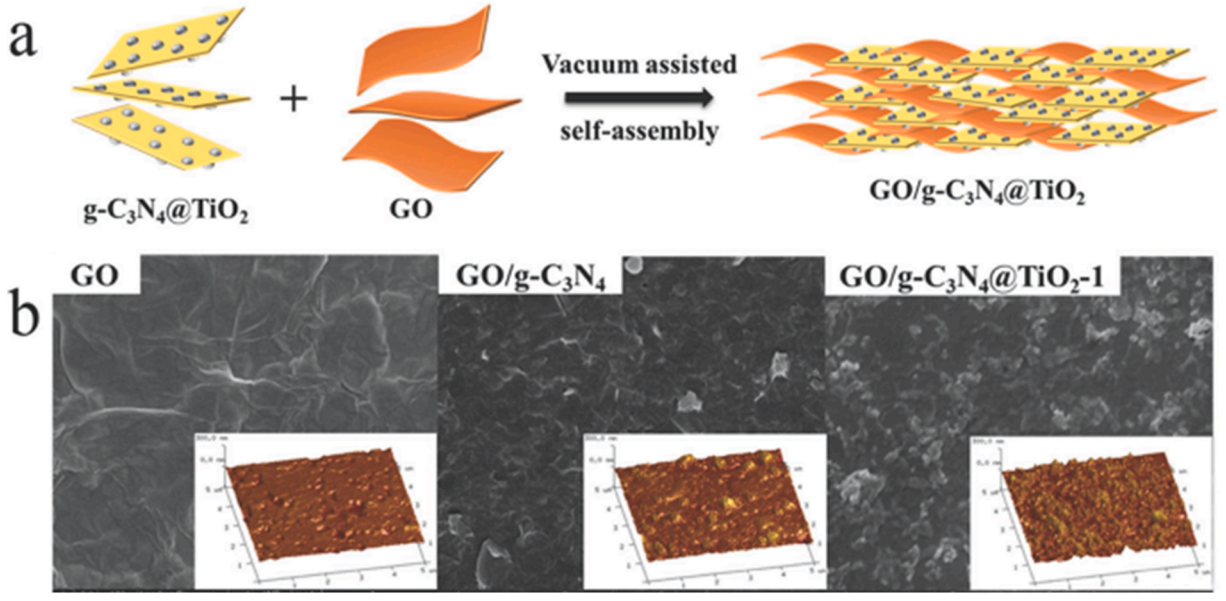

Fig. 9. Schematic description of the synthesis of GO/g-C_3N_4@TiO_2 via vacuum assisted self-assembly (a) AFM and SEM images of GO, g-C_3N_4@TiO_2 and GO/g-C_3N_4 @TiO_2 (b) [53].

CdS/g-C_3N_4/rGO concurrently decomposed foulants and inactivated the microorganisms by sunlight. Reactive species produced on modified CdS/g-C_3N_4/rGO membrane might be primarily responsible for the breakdown of foulants and the inactivation of associated microorganisms [59].

2. 3. Applications of g-C_3N_4 based membranes

2.1. 3.1 Elimination of organic dyes

Environmentalists are concerned about the industrial wastewater that is the primary cause of organic dyes globally, which might negatively influence aquatic ecosystems. Among the frequent organic components found in dyeing wastewater are the dyes. They have been identified as genotoxicants with their potential to cause birth abnormalities and food chain concerns. Traditional membranes have a limited capacity to filter out color molecules that have smaller size than the membrane's pore sizes. When filtration is carried out for long-term, the fouling of membranes appears as a major issue and requires attention [60].

g–C_3N_4–based membranes have been investigated frequently for their use in wastewater treatment to address these issues. A summary of recent advancements in the manufacturing and functioning of g–C_3N_4–based membranes for extracting dissolved dyes without light are shown in Table 1. Using artificial nanopores and spacers, Wang et al. created GCNS that were subsequently integrated into the surfaces of anodic aluminum oxide (AAO) membranes using vacuum filtration. It was showed that spacers between partly exfoliated g-C_3N_4 and mesoporous structure might operate as nanopores for water transport, but the system rejected bigger particles [38]. Aside from that, the nanochannels were robust at various pH levels (1–11) and pressure (up to 6 bars). Compared to pristine polyethersulfone (PES) membranes, the obtained membrane demonstrated increased rejection efficiency for RhB and EB (75.5% and 87.2%, respectively). The outcomes of this study were used to create a new $Fe(OH)_3$/g-C_3N_4 membrane, which was attained using vacuum filtration and suction evaporation. The membrane was capable of removing 99.9% of EB molecules from a solution containing 10 mgL^{-1} of EB [61]. For elevated pressure (<3 bar), new fractures or holes were formed in the membranes, resulting in a drop in the rejection rate and rise in the water flux. Due to their specific physicochemical characteristics, metals and metal oxides nanoparticles have been reported in previous research to promote the formation of nanostructured membranes (Yin and Deng, 2015). Similarly, membrane developed from sulfonated poly (2,6-dimethyl-1,4-phenylene oxide)/g-C_3N_4 showed an extraordinary water flux of 8867 L m^{-2} bar^{-1} and rejection rates of 89%, 84%, and 100% towards EB, RhB, and MB, respectively. The acid-base pairings formed by the basic sites of g-C_3N_4 and SO_3H allowed the 2D nanochannels to remain enduring under variable pH and high pressure [62].

Similarly, Wang et al. observed the increased tensile strength of the membrane when he added polyacrylic acid (PAA) into a GCNS solution prior to depositing it to the surface of polycarbonate (PC) membrane [65]. It has been claimed that the inclusion of suitable spacers could result in increased interlayer distances [66]. The addition of PAA into the membrane resulted in bigger nanochannels and spaces. Comparing the previous studies, the water flux was significantly increased (from 29.5 to 112 L m^{-2} bar $^{-1}$), but the rejection

Table 1
Elimination of organic dyes by g-C_3N_4 based membranes without light radiations.

Substrate	Membrane	Synthesis Technique	Pollutant	Concentration (mg/L)	Rejection (%)	Pressure (bar)	Permeance (LMH/bar)	Ref.
AAO	GCNS	Vacuum filtration	EB	10	87.2	1	4526	[38]
			RhB		75		29.5	
	$Fe(OH)_3$/GCNS		EB	10	99	1	27.5	[61]
PC	PAA/GCNS		RhB	10	52	1	105	[39]
			EB		83		112	
PVDF	(SPPO)/GCNS		EB	10–50 μmol/L	100	1	49	[62]
			RhB		100		38	
			MB		100		49	
	MB/GCNS		EB		98	1	2226	
			RhB		78 ± 5		1423	
			MB		100		1757	
	EB/GCNS		EB		97	1	1391	
			RhB		99		557	
			MB		100		1908	
	SPPO/GCNS		EB		89	1	2386	
			RhB		84 ± 1		1638	
			MB		100		2783	
HPAN	PDA/PEI/GCNS	Oxygen plasma, bio-inspired	Reactive dyes	/	~97	4	~18	[63]
	PDA/PEI/GCNS	co-deposition	RhB	/	99.8		23.7	
					70		42	
PES	/	/	EB	10	0	1	24,458	[64]
	GO	Vacuum filtration			94.9		7.7	
	GO/GCNS				95.5		15.4	
MCE	GO		MB	20	32.8	1	26.6	[58]
	GO/GCNS				64.9		7.6	
	Gly-GO/GCNS/HPEI	Vacuum filtration, dip coating			90		25.8	

efficiency for RhB and EB remained 83% and 52% resectively [65]. In a separate study, GCNS were inserted into a polyamide layer to increase the water permeability of the layer. Ye et al. used oxygen plasma to create GCNS and placed it onto the hydrolyzed polyacrylonitrile substrate with a polyethylenimine (PEI)/polydopamine (PDA) layer. The wettability of the GCNS with oxygen plasma treatment was enhanced, resulting in a strong antifouling characteristic. The constructed membrane rejected reactive dyes (98.5%) having molecular weights from 610 to 630 Da and a water flux of 23.7 L m^{-2} bar $^{-1}$ with a rejection rate of 98.5% [67]. Additionally, it has been demonstrated that introducing g-C_3N_4 into graphene oxides (GO) causes to increase the membranes nanochannels. Liu et al. used vacuum filtration to construct GCNS-intercalated GO membranes to increase the permeability of the membranes. The GO/g-C_3N_4 membrane exhibited water flux double to that of pure GO membranes. The increasing quantity of corrugations or wrinkles in the membranes, which resulted in the formation of additional nanochannels in the membranes, may have contributed to the rise in water

Table 2
Recent developments in the synthesis and organic dyes elimination efficiency of g-C_3N_4 based membranes under light irradiation.

Membrane substrate	Membrane	Fabrication method	Pollutant	Concentration (mgL^{-1})	Radiations	Performance	(Rate: %)	Ref.
PAN	PAN/Protonated GCNS	Vacuum filtration, dip coating	MB	200	Visible light	Rejection	99.83%	[44]
CCP	GCNS/CCP	Chemical vapor deposition, plasma treatment		10	Xe lamp, λ >400 nm	Removal	60%	[56]
AAO	GCNS	Vacuum filtration		16	Mercury lamp, λ > 400 nm		100%	[71]
CA	CA/β-CD/GCNS			6.4	Visible light		99.7%	[69]
PTFE	TiO_2/PAA/PTFE g-C_3N_4/TiO_2/PAA/PTFE	Plasma-enhanced surface graft, self-assembly		10	Xe lamp, λ >400 nm	Degradation	40% 78%	[10]
PVDF	PVDF/GCNS MCU-C_3N_4	/ Vacuum filtration	RhB	5	/ Xe lamp, λ >420 nm	Adsorption Degradation	10% 84.24%	[68]
PVDF	/				Xe lamp, λ > 420 nm		10%	[44]
	PVDF/Fe_3O_4/GCNS	Magnetically induced freezing casting					97.8%	
PES			MO	10	Xe lamp, λ >400 nm		0%	[72, 73]
PES	PES/Ag/g-C_3N_4	Phase inversion					77%	
Nafion	Nafion/Ag/g-C_3N_4	Vacuum drying	RhB		Xe lamp, λ >420 nm		86%	[74]
PC	Fe-POMs/g-C_3N_4	Vacuum filtration	MB Congo red RhB COD	 290	100 mW cm^{-2}	Rejection	99.1% 98.6% 50.4% 43%	[75]
PAN	Chitosan/FeOOH/g-C_3N_4	Electrospinning, Dip coating	MB	50	Xe lamp, λ >400 nm	Removal	68.49%	[76]
PVDF	/ PVDF/g-C_3N_4 PVDF/Ag_3PO_4/g-C_3N_4 NH_2–Ag_3PO_4/GCNS	/ Phase inversion	RhB	10	Xe lamp, λ > 420 nm	Degradation	41% 85% 98% 18%	[77]
PTFE	TiO_2/PAA/PTFE	Plasma-enhanced surface graft, self-assembly	MB		Xe lamp, λ >400 nm	Degradation	40%	[10]
TiO_2 nanotube array	TNA/g-C_3N_4/QDs	Potentiostatic anodization	RhB	3	Xe lamp, λ >400 nm	Removal	60%	[47]
CA	RGO/GCNS P25	Filtration		5	100 mW cm^{-2}, λ > 400 nm		60% 32%	[78]
PVDF	GO/PDDA GO/PDDA/g-C_3N_4	Vacuum filtration		10	Xe lamp, λ > 420 nm		97.68% 94.17%	[79]
CA	RGO RGO/GCNS RGO/g-C_3N_4nanotube	Vacuum filtration annealing			Xe lamp, λ > 420 nm		99% 97.50% 96.10% 95%	[80]
PC	GO/gold NPs/g-C_3N_4	Vacuum filtration	R6G	4.8	Xe lamp, λ > 400 nm	Degradation	100%	[81]

permeance. Furthermore, the anti-pressure ability was significantly improved even when the pressure was as low as 5 bars because the nanochannels were stiff due to the assistance of GCNS [64]. Polymers were further incorporated into GO and g-C_3N_4 membranes in a later phase. Applying the vacuum filtration and coating techniques, Wu et al. developed a series of glycine/hyperbranched polyethyleneimine induced GO/g-C_3N_4 lamellar membranes. Both glycine and g-C_3N_4 effectively increased the spaces between the layers of membranes; however, the former resulted in wider channels, while the latter resulted in smaller nanochannels. The composite membrane exhibited equal water permeation of 25.8 L m^{-2} bar^{-1} and a much higher rejection rate of 90% for MB (20 mgL^{-1}) at pH 10. But, at pH 4, the rejection rate reduced to 30% that might be endorsed to the chemical etching of the lattice of the membrane. Although g-C_3N_4 based materials increased the separation efficiency of the membrane, but the photocatalytic properties of g-C_3N_4 were not fully exploited in these studies [58].

Since, g-C_3N_4 has low bandgap and exhibits sufficient photocatalytic activity. The pollutants, adhering to the surface of g–C_3N_4–based membranes are deteriorated under light irradiations. Hence a reduction in pore blockage and an increase in the self-cleaning capabilities of the membranes occur. Various functionalized g-C_3N_4 materials have been created and employed as modifiers for membrane because the efficiency of pristine g-C_3N_4 is limited by the electron-hole pairs recombination under visible-radiations. A summary of recent advances in the synthesis of g-C_3N_4 based membranes and their photocatalytic efficiency against organic dyes is presented in Table 2. Dou et al. used chemical vapor deposition (CVD) to deposit GCNS onto cellulose-based carbon papers (CCP), treated it with oxygen plasma to improve the wettability. Within 3 h of visible light exposure, the GCNS/CCP membrane removed <60% of MB (10 mg L^{-1}) from the water sample. The GCNS/CCP membrane maintained constant degradation efficiency even after five cycles [56].

Similarly, Huang et al. fabricated (DMSO)-C_3N_4 using urea, cyanuric acid, and melamine (MCU) precursors. Then he applied vacuum filtration to immobilize (DMSO)-C_3N_4 on polyvinylidene fluoride (PVDF) membranes. The resultant membrane revealed eight times more dyes degradation efficiency than the simple PVDF membrane. A four-stage filtering system was employed to test the antifouling aptitudes of photocatalytic membranes, and the results showed that when exposed to visible light for 30 min, the flux recovery ratio (FRR) of MCU- C_3N_4/PVDF membranes reached above 80% [68]. On the other hand, 30 min of visible-light irradiation may accelerate membrane fouling. Later research discovered that following a period of visible-light irradiation, contaminated membrane separation efficacy may be recovered [44,69]. Using a simple filtration of GCNS onto porous polyacrylonitrile (PAN) substrates, Li et al. built PAN membrane surfaces having self-cleaning and antibacterial characteristics. The functionalized g-C_3N_4 membrane rejected 99.83% of MB (200 mg L^{-1}). Furthermore, it was shown that exposing it to visible light for 60 min could primarily recover its initial permeability. In addition, the g-C_3N_4 membrane had superior antibacterial activity against *E. coli* compared to membranes that did not contain g-C_3N_4 [70]. In a similar way, Liu et al. produced g–C_3N_4–based membranes that were functionalized with β-cyclodextrin using cellulose acetate substrate. On exposing to visible light, the membrane removed 99% of the MB (6.4 mg L^{-1}) from the water. Appreciably, the utilized membrane could regain its original color by exposing to visible-light for 60 min and can be reused for five times without losing its efficiency. The research also revealed that OH and electron were key players in MB disintegration [69]. The dye erasure efficacy of g-C_3N_4 based membranes might be enhanced by including additional resources regardless the benefits of the inclusion of exfoliated or synthesized and characterized g-C_3N_4. Several investigations have revealed that silver (Ag) nanoparticles can boost the photocatalytic activity of g-C_3N_4 by decreasing the electron-hole pair recombination and increasing the surface plasmon resonance [72,73]. Phase inversion was used by Zhang et al. to introduce silver-altered g-C_3N_4 into PES films. The hybrid membranes' water flux was around three times greater than that of the pure PES membranes. Furthermore, the increased hydrophilicity and photo-degradation abilities were attributed to the increase in FRR (41–87%) [72,73]. Similarly, silver nanocrystals were used by Zhang et al. to modify g-C_3N_4/Nafion membranes (AgNCs). Photocatalytic activity and recyclibilty of the resultant composite membrane toward RhB were better compared to the g-C_3N_4/Nafion membranes. Furthermore, semiconductor materials were recommended to be used to create versatile g-C_3N_4 based membranes [74]. Ag_3PO_4, for example, was considered a strong contender to modify g-C_3N_4 based membranes due to its advantageous band location [82]. A phase-inversion approach was used to create Ag_3PO_4/g-C_3N_4/PVDF membranes by Cui et al. Because of the decreased surface roughness and increased porosity of the Ag_3PO_4/g-C_3N_4/PVDF membranes, they were able to produce twice as much clean water as with the PVDF or g-C_3N_4/PVDF membranes. The rate of degradation (85%) of RhB (10 mg L^{-1}) by g-C_3N_4/PVDF had increased to 98% by the modified membrane [77]. Other than g-C_3N_4 combinations with Ag_3PO_4, the formation of hybrid membranes with TiO_2/g-C_3N_4 may also increase the anti-fouling, hydrophilic and light absorption activities [83,84]. By employing plasma-enriched surface implanting and PAA as the bridging agent, Chi et al. fixed TiO_2/g-C_3N_4 onto PTFE films. The water permeability of TiO_2/PAA/PTFE and g-C_3N_4/TiO_2/PAA/PTFE membranes was proximately same, but the degrading proficiency was substantially greater (78%) for g-C_3N_4/TiO_2/PAA/PTFE. This might be ascribed to the proper integration of TiO_2 into g-C_3N_4 [10].

The dye sensitizing effects may have been generated by the development of g-C_3N_4/TiO_2 heterostructure. Furthermore, the FRR was greater for g-C_3N_4/TiO_2/PAA/PTFE (100%) than TiO_2/PAA/PTFE membranes (59%) just after 15 min of exposure to UV or visible light. This was the first time that potentiostatic anodization was used to immobilize g-C_3N_4 specks into a freestanding TiO_2 nanotube array (TNA) membrane. Straight nanochannels and well-ordered patterns were seen in the TNA membrane. Due to the same water flow of the TNA and g-C_3N_4/TNA membrane, it was concluded that the effects of the g-C_3N_4 dots on the water permeability may be ignored. In dark, the g-C_3N_4/TNA membrane was unable to degrade RhB, however under visible radiations successfully removed (>60%) RhB (3 mg L^{-1}) [47]. Not only the nanosilver and semiconductor materials were considered for enhancing the functioning of g-C_3N_4 base membranes, but the integration of Fe_3O_4 NPs were also counted as effective agents to increase the functioning of the modified membranes [70,75]. Magnetically stimulated freeze casting was suggested by Li et al. for the construction of Fe_3O_4/g-C_3N_4/PVDF films. To build an ordered lattice structure, g-C_3N_4 mixtures were modified with magnetic Fe_3O_4 that may travel to the membrane exterior in the magnetic field direction. The images of the self-designed cyclic degradation system and macroscopic sketch of a

probable dye degradation mechanism over FCMs are shown in (Fig. 10) [70].

Likely, the high photodegradation efficiency (10–97.8% against RhB) of the Fe_3O_4/g-C_3N_4/PVDF films is due to the high light infiltration and a large quantity of photocatalytic action spots. In comparison to ordinary fusion membranes (1300 L m^2 bar^{-1}), the water flux was extremely better 15,000 L m^2 bar^{-1}. These membranes, on the other hand, had a restricted contact surface with pollutants, which resulted in reduced photocatalytic activity. The application of visible photo-controlled catalysis and other oxidation tools for membrane cleaning was a novel approach [70]. Using C_3N_4 sol as precursor and the Fe-comprising polyoxometalates (Fe-POMs) were employed as a molecular binder in the formation of photo-Fenton membranes by Lan et al. The resultant membranes exhibited good water permeation and efficiently rejected the pollutant molecules. In the presence of H_2O_2, the contaminated membrane degraded attached MB dyes within 80 min under visible radiations [75].

Electrospinning and dip coating was used by Zheng et al. to create a highly hydrophilic CS/PAN@FeOOH/g-C_3N_4 film [76]. The water flux of the membrane, contaminated with MB and erythromycin, was resorted successfully when membrane was assisted with photo-Fenton reaction. The MB removal yields by the membrane were 62.7% under visible radiations, 59.1% in darkness, and 68.49% with photo-Fenton assisted reaction respectively. g-C_3N_4 base membranes containing g-C_3N_4/GO heterojunction were frequently used to remove dye from contaminated water [85]. Polydimethyl diallyl ammonium chloride (PDDA) was used a membrane surface transformer to create GO/PDDA/g-C_3N_4 membranes. GO/PDDA/g-C_3N_4 membranes showed higher water fluxes (8.24–16.97 L m^2 bar^{-1}) but significantly lower efficacy in removing RhB (10 mg L^{-1}) (97.68–94.17%) [79]. Zhang et al. constructed a multi-functional membrane using GCNS, CNTs, TiO_2 nano-sheets, and GO sheets to further improve the degradation efficiency. Under visible-light irradiation, the GO/TiO_2-CNT/GCNS membranes removed >95% of MO [86]. The photogenerated electrons via revulsion of similar charged molecules might not only contribute to photodegradation but also increase MO removal efficiency. To detect and remove organic dyes, Qu et al. created a multi-purpose membrane by introducing gold nano-particles and g-C_3N_4 into GO nano-sheets. The created a multi-purpose membrane with outstanding photodegradation capacity was able to fully degrade Rhodamine 6G (R6G) in 2 h using. In contrast to other membranes, this membrane detected R6G with a detection limit of 5.0×10^{-14} M [81]. To diminish the recombination ratio of electron-hole pairs created by g-C_3N_4 based membranes, RGO that is essentially derived from GO, might be used as an electron acceptor [87]. Chinese researchers in 2016 built RGO/CA/CNNS employing RGO and CNNS on CA membrane. The membrane filtration in combination with photocatalysis exhibited greater water permeability and RhB exclusion efficiency. Nearly four times more RhB molecules were eliminated under visible radiation than as in membrane without light irradiation. As a result, photocatalytic degradation was primarily liable for the enriched removal efficiency of the membrane. g-C_3N_4 nano-tube interpolated RGO membranes were created by Wei et al. using vacuum-assisted filtering. The observed water permeability of RhB solution was excellent for CNNS/RGO than for RGO and CNNS [80].

In order to enhance the elimination efficiency of the g-C_3N_4 based membranes against the colored toxin, various new photocatalytic membrane reactors (PMR) were constructed in research labs. A photoreactor based on g-C_3N_4 was developed by Zhou et al. which exhibited 2 mLh^{-1} of dye solution flow rate during the photo-degradation test in the lab. In other words, the g-C_3N_4 reactor was very effective in degrading rhodamine, Sudan orange G, MB (18.4, 10.7 and 16.0 mgL^{-1}) with removal rates close to 100% [78].

Hu et al. created an efficient PMR by combining a Al_2O_3 hollow fiber sheath unit with P-doped g-C_3N_4 photocatalyst coated on Al_2O_3 substrate (Fig. 11) [88]. P-doping of g-C_3N_4 supported the filling of C vacancies which in turn facilitated the repair of structural flaws of the membrane and significantly decreased charge recombination. When this PMR was utilized up to four cycles, it maintained

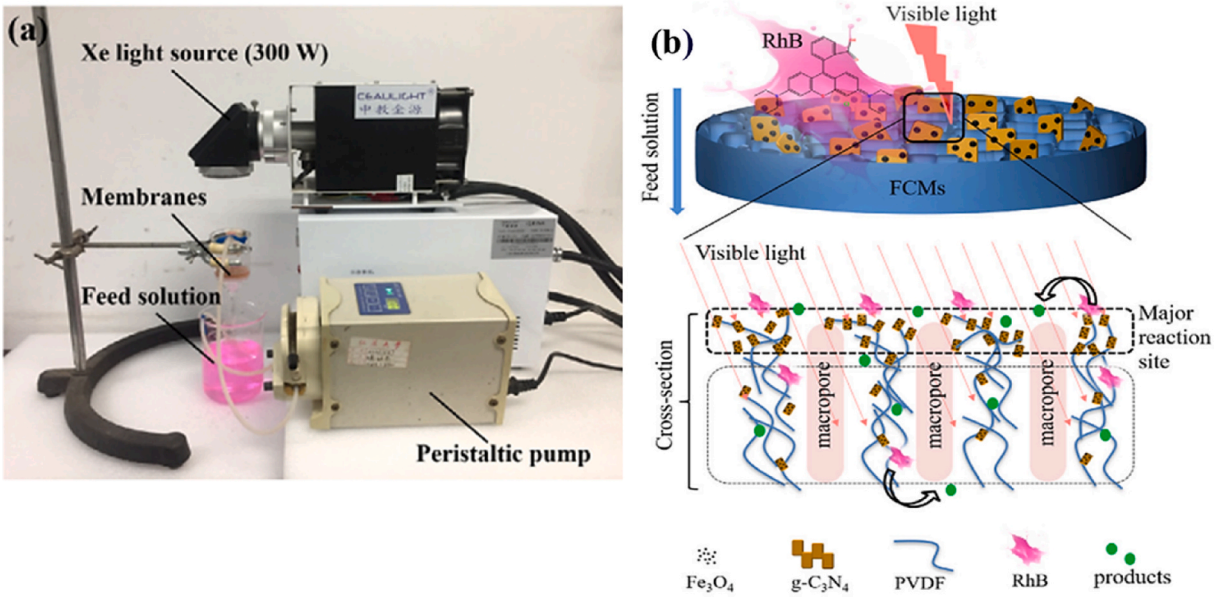

Fig. 10. Self-designed cyclic degradation system (a) macroscopic sketch of the probable mechanism of degradation of dye over FCMs (b) [70].

a high degrading efficiency of MB (>90%) [88].

2.2. 2 Elimination of phenolic compounds

In terms of environmental protection and human health, it is critical to remove phenols before they may be discharged into the atmosphere [89]. For their exceptional performance, hybrid membranes using g-C_3N_4 and photocatalytic technologies have received a lot of attention. g-C_3N_4 based hybrid membrane have made significant advancements in construction and performance for elimination of phenolic chemicals (Table 3). With the use of TiO_2, GO, CNTs, and g-C_3N_4, Zhang et al. shaped photo-abetted nano-filtration membranes. The GO/CN/TiO_2-CNT membrane was able to remove over 80% of BPA under laser illumination, which is almost twice as much as membrane filtration alone. An additional benefit of this membrane was its high regeneration and filtration stability [86]. Salim et al. reformed the PES membrane with oxygen-doped g-C_3N_4 and hydrophilic surface modifying macromolecules (LSMM) to intensify the active sites accessible to the light source. To ease the dispersion of g-C_3N_4 over the membrane surface, the LSMM was predominantly composed of Al_2O_3, SO_3, and SiO_2.

They studied the influence of LSMM loading on permeate flux to further improve the efficiency [90]. The photocatalytic efficiency of the g-C_3N_4 based membrane might be enhanced by loading LSMM that increases the light absorbency of g-C_3N_4. The phenol (10 mg L^{-1}) degradation rate was raised to 35.8% when hybrid membrane was subjected to the UV irradiation, which was predominantly due to photo-degradation rather than physical size sieving [91]. Other techniques i.e., unconventional oxidation procedures (UOP) and photo-electrocatalytic (PEC) technique were integrated with membrane separation to increase the efficacy of g-C_3N_4 based membranes for degradation of phenolic compounds. GCNS was used by Chen et al. to attach Mn_3O_4 nanodots employing vacuum filtration to produce Mn_3O_4/GCNS/PTFE membranes. The peroxymonosulfate (PMS)-based AOP might be triggered by Mn_3O_4 to eliminate organic contaminants effectively in this system, where g-C_3N_4 served as a linker between active fragments and membranes. The recyclability and stability test were carried out to check the usability of the membrane. Even after five uses, 4-CP elimination rates might still reach 80% in 60 min. This demonstrated that even after use, the catalytic membrane still exhibited strong catalytic activity. In order to improve the catalytic performance of cycled catalytic membrane, the membrane was thermally treated at 150 °C for 3 h with reacting with ethanol. It was found the catalytic performance of cycled membrane was improved to 88%, which suggested the catalytic membrane possesses potential application prospects in the field of pollutant removal [95]. Degradation of p-chloroprene (4-CP) was over 90% in the Mn_3O_4/GCNS/PTFE sheets containing one mM PMS, whereas only 10% of 4-CP was adsorbed by original PTFE film. The perylene imide (PI)/g-C_3N_4 membranes synthesized were fabricated via liquid-based method by employing SiO_2 membranes as supports. The membranes were able to break down 100% BPA within 30 min when exposed to PMS and visible light as shown in Fig. 12(a–c) [93]. Similarly, Wang et al. used the PEC approach with membrane filtering under visible-light to remove phenol. They applied CNTs as conductive material on Al_2O_3 membranes and g-C_3N_4 as photocatalytic layers on the CNTs [94]. The PEC method, which uses an external voltage to separate electron-hole pairs across the photocatalysts, might improve the catalytic efficacy [96,97]. In addition, PEC may lead to repulsive forces and electrochemical oxidation, which are advantageous for the deterioration of contaminants [98]. The extraction of phenol (5 mg L^{-1}) was raised to 94% when light illumination and 1.5 V external voltages were used together, as compared to just 7% solely for membrane filtration and 26% for visible-light illumination (Fig. 13(a–c) [98].

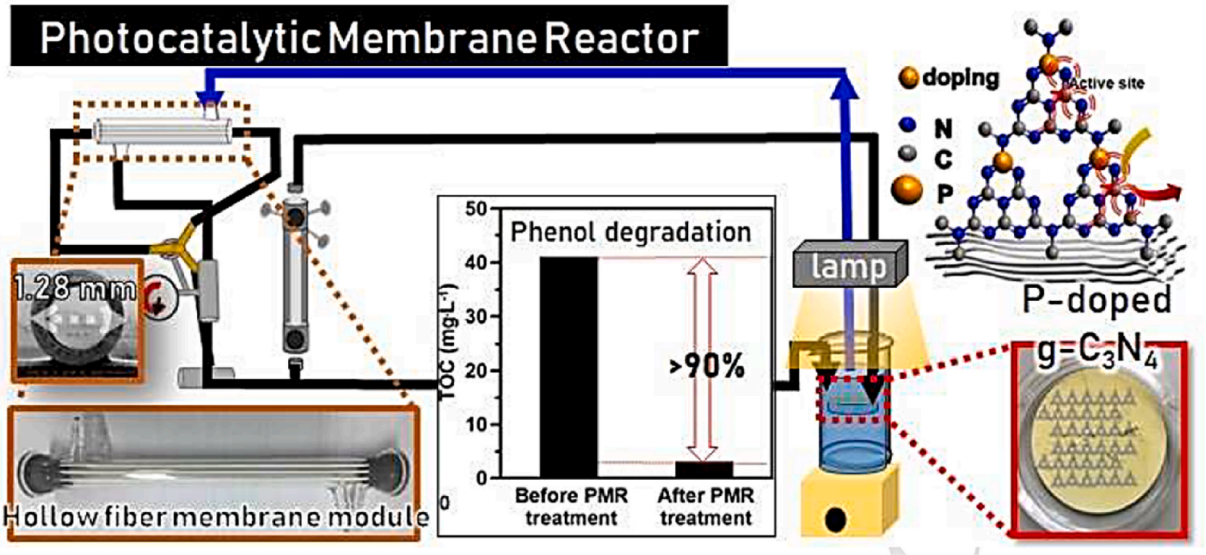

Fig. 11. Illustration of the functioning of photocatalytic membrane reactor integrated with P-g-C_3N_4 with Al_2O_3 hollow fiber sheath unit [88].

Table 3
Recent advances in elimination of phenolic compounds by g-C_3N_4 based membranes.

Membrane substrate	Modifier	Fabrication method	Pollutant	Concentration (mg/L)	Radiations	Performance	(Rate: %)	Ref.
Alumina	GO/GCNS/ TiO-CNT	Vacuum filtration, annealing	Bisphenol A		100 mW cm^{-2}	Rejection Removal	40% 82%	[86]
PES	/ O-g-C_3N_4/ LSMM	/ Phase inversion	Phenol	10	UV	Adsorption Degradation	0.52% 35.8% 35%	[90] [91]
PTFE	/ Mn_3O_4/GCNS	Vacuum filtration	Chlorophenol	12.8		Adsorption Degradation	10% 90%	[92]
SiO_2	Perylene imide/g-C_3N_4	Calcination	Bisphenol A	10	Xe lamp, $\lambda > 420$ nm		100%	[93]
Al_2O_3	CNTs/g-C_3N_4	Vacuum filtration, dip-coating	Phenol	5		Removal	26% 94%	[94]

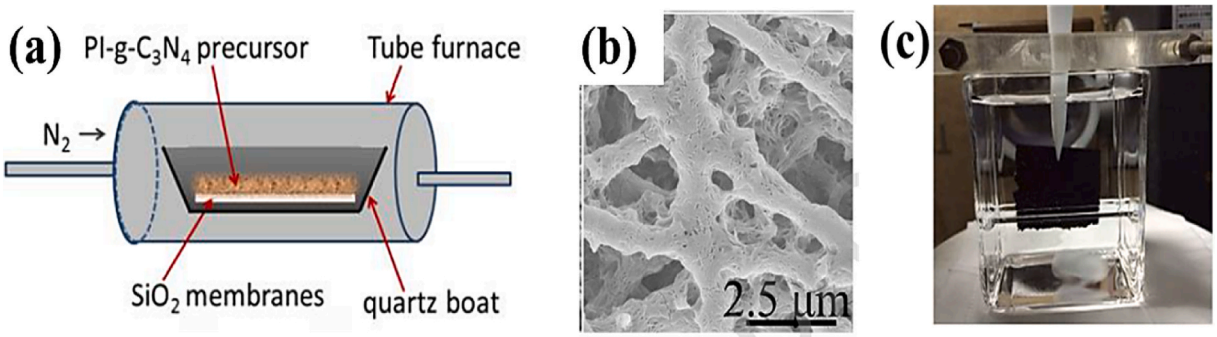

Fig. 12. Illustration of the preparation (a) an optical image (b) and SEM images of PI-g-C_3N_4 membranes (c) [93].

2.3. Removal of pharmaceuticals

Pharmaceuticals are an integral part for healthy life. Due to the development of novel and infectious diseases, the use of pharmaceuticals has been increasing. The pharmaceutical wastes are discharged without proper treatment from hospitals and farms, and thus posing a hazard to aquatic life and human health [99,100]. Pharmaceutical wastewater has a high concentration of antibiotics, which may be difficult to remove. Antibiotics such as sulfamethoxazole (SMX) and tetra-cycline hydrochloride (TCH) are widely utilized in food sector, animal husbandry and aquaculture as antimicrobial medications [101]. Photocatalytic membrane (PM) technique, which blends the benefits of membrane separation with photo-catalysis, had been viewed as a viable methodology to pharmaceutical wastewater treatment [80,102]. The photocatalytic activity of PMs modified with nanomaterials, such as g-C_3N_4 nanoparticles and g-C_3N_4 nanocomposites, against pharmaceuticals under visible light has been shown. Membranes may also benefit from the high-water flow and anti-fouling characteristics of the g-C_3N_4 based nanoparticles at the same time. Table 4 outlines the progress made in the manufacturing and efficiency of g-C_3N_4 based membranes for elimination of drugs and medicines. To photodegrade tetracycline hydrochloride (TCH), Huang et al. used a vacuum filtering approach to immobilize g-C_3N_4 onto PVDF membranes to develop (melamine, cyanuric acid, urea) MCU-C_3N_4/PVDF. The hybrid membrane showed 70% increase in TCH breakdown efficiency compared to the original membrane. Within half hour of visible radiation, the FRR had risen to above 90%, proving the increased self-cleaning ability of the membrane used (Fig. 14) [68]. The increasing concentration of g-C_3N_4 caused to develop a GCNS, which in turn decreased the water permeability. Yet the degradation efficacy was increased by 70%, still the issue of fast recombination of electron-hole in g-C_3N_4 was to be resolved [54,103]. Electrospinning and heat polymerization was used to create g-C_3N_4/Co–TiO_2 nanofibrous membranes by Song et al. The TCH degradation efficiency of the hybrid membranes was 90.8% after 60 min of exposure to visible light. In addition, the hybrid membranes reduced bacterial numbers by six logarithms in only 60 min. A similar approach was used in the degradation of SMX by Yu et al. who created meso-porous g-C_3N_4/TiO_2 nanocomposites and incorporated them onto PSF substrata. The nanocomposites exhibited improved removal efficiency (14%–69%), with a reduction in water fluidity (628.6–551.2 LMH/bar), compared to original PSF membranes. Since no photocatalyst was identified in the mixture, the rate of photodegradation remained nearly constant throughout the 30-h test [30]. It's possible that the breakdown of chemical bindings caused by hydroxyl radicals and UV irradiation reduced the tensile strength to some degree. An effective tactic for addressing the recombination issue of g-C_3N_4 is to combine it with substances like carbon nanotubes (CNT) and graphene oxide (GO) [104,105] Coalescence of light generated electron-hole pairs caused by g-C_3N_4 was prevented by using N-CNT and GO as electron-seizure agents. Additionally, the enrichment and degradation rates of O-g-C_3N_4/GO/N-CNT membranes were exhibited for tetracycline hydrochloride and were reported to be up to 96.64% and 94.30%, respectively. When their reusability was assessed, no discernible enrichment or catalytic

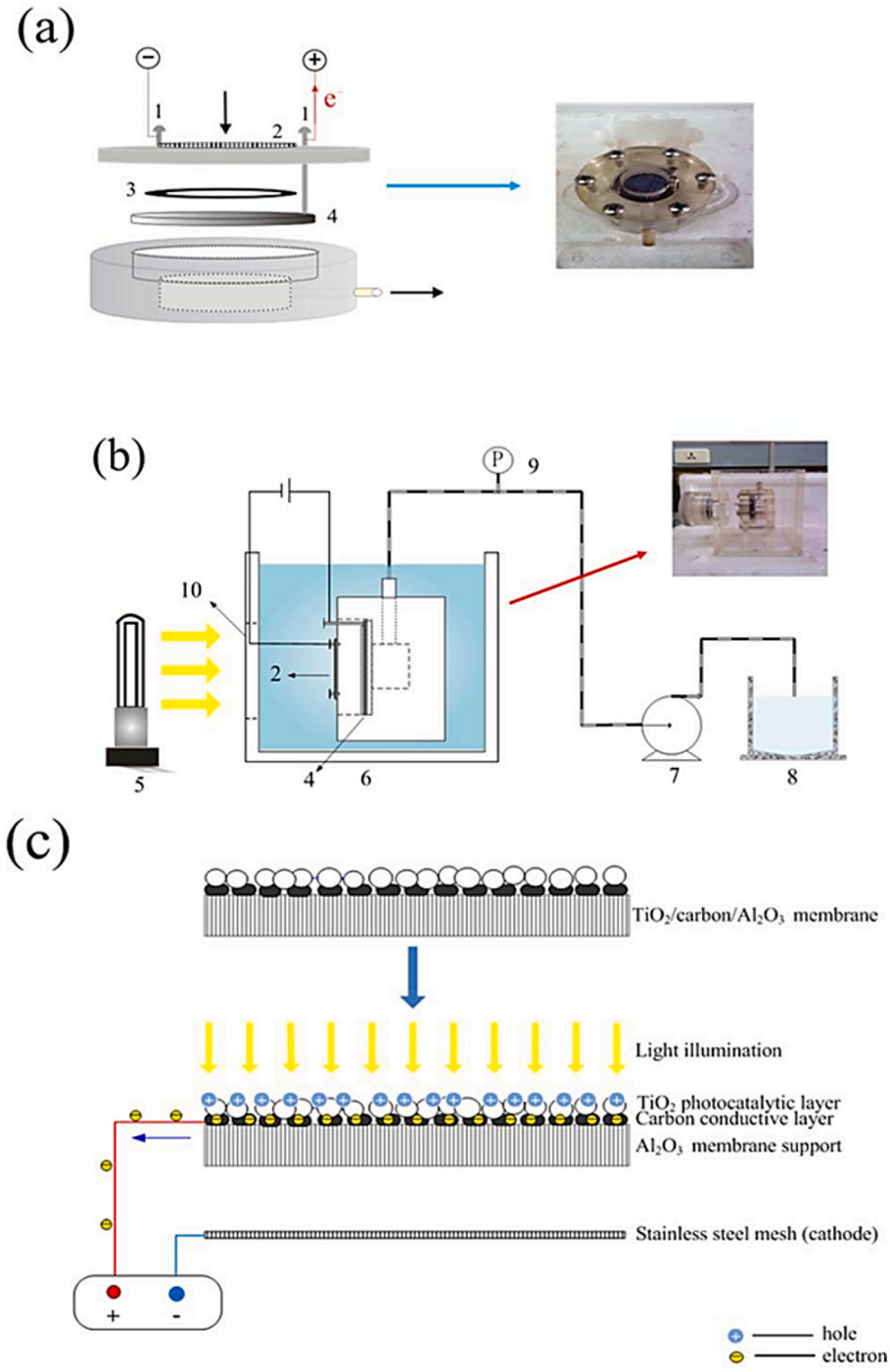

Fig. 13. Photoelectrocatalytic membrane module (a) lab-scale photoelectrocatalytic membrane system (b) schematic diagram of photo-electrocatalytic membrane (c) [98].

activity decline was seen. These findings proposed a novel method for the highly effective removal of environmental pollutants using recyclable O-g-C_3N_4/GO/N-CNT membranes.

2.4. Removal of other pollutants

The impurities like oil, dyes and heavy metals, as described above, are mutagenic, immunogenic and carcinogenic. Due to these properties these are hazardous pollutants and can pollute our water reservoirs ecology [106,107]. Diverse g-C_3N_4 based membranes

Table 4
Removal of pharmaceuticals by g-C_3N_4 based membranes.

Membrane substrate	Modifier	Fabrication method	Pollutant	Concentration (mg/L)	Radiations	Performance	Rate	Ref.
PVDF	/	/	TCH	5	Xe lamp,	Degradation	~1%	[68]
	MCU-C_3N_4	Vacuum filtration			$\lambda > 420$ nm		71.26%	
PC	O-g-C_3N_4/ GO/N-CNT			20			94.30%	[104]
Co–TiO_2	/	/					36.90%	[54]
	g-C_3N_4	Electrospinning, thermal polymerization					90.80%	
PSF	/	Phase inversion	SMX	10		Removal	14%	[30]
	g-C_3N_4/TiO_2						69%	
PTFE	Mn_3O_4/GCNS	Vacuum filtration	Levofloxacin				50%	[92]
Alumina	GO/GCNS/ TiO-CNT		SMX		100 mW cm^{-2}		82%	[86]

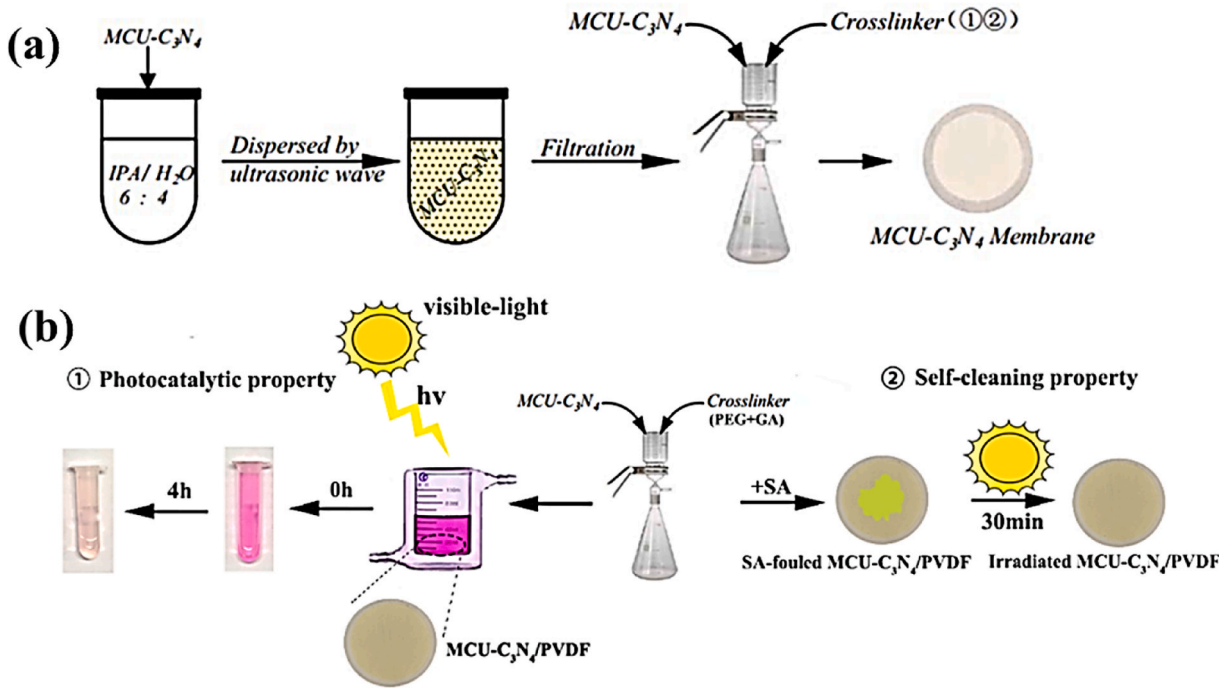

Fig. 14. The synthesis process (a) photocatalytic and self-cleaning ability of MCU-C_3N_4/PVDF membranes (b) [68].

have been established and used to for wastewater treatment. An improved + ve charged NF membrane has been developed by Bi et al. using the PDA and modified g-C_3N_4. The membrane demonstrated substantial divalent cations rejection (Ba^{2+}, Cu^{2+}, and Zn^{2+}) as well as outstanding antifouling properties. Because of the hybrid membrane's improved hydrophilicity, the PAD-g-C_3N_4 was effective in increasing water flux, especially for divalent ions [108]. Alternating capturing and releasing of the target ions might be accomplished by using electrochemically switched ion exchange [24,109]. This method was successful in separating low concentration targets quickly and efficiently. The ion absorption and release, on the other hand, have to be done independently in this method. To get around this problem, Gao et al. presented an improved system, which is an electrochemical reaction switched ion permselectivity (ESIP) [110]. A 3D porous carbon membrane (g-C_3N_4@MWCNTs) was manufactured and attached to the PTFE membrane using pressure filtering by Gao et al. Due to the capillary tunnel effect of composite membrane, the system has a high flux of 10 g m^{-2} h^{-1} and current performance (38%) for continual Zn^{2+} removal with high consistency under ideal operation conditions, as indicated in Fig. 15 (a, b) [110].

The fouling of the hybrid membranes occurred by the formation of thick oily layers on the surfaces of g-C_3N_4 based membranes during their applications for oily wastewater treatment. A reduction in fouling was achieved by photo-degradation assisted filtration by hybrid membranes. For instance, Alias et al. used electrospinning to create g-C_3N_4/PAN nanofiber-covered alumina films for oil field-generated water (OPW) treatment. Elevated water affinity, thin mesh structures, and even nanofiber structure of the g-C_3N_4/PAN membranes resulted in more OPW flow and oil rejections than the initial alumina membranes. Another benefit of using the nanofiber coating is that it prevented the membrane surface fouling due to the excellent adsorption of OPW [48]. The addition of g-C_3N_4 gave the

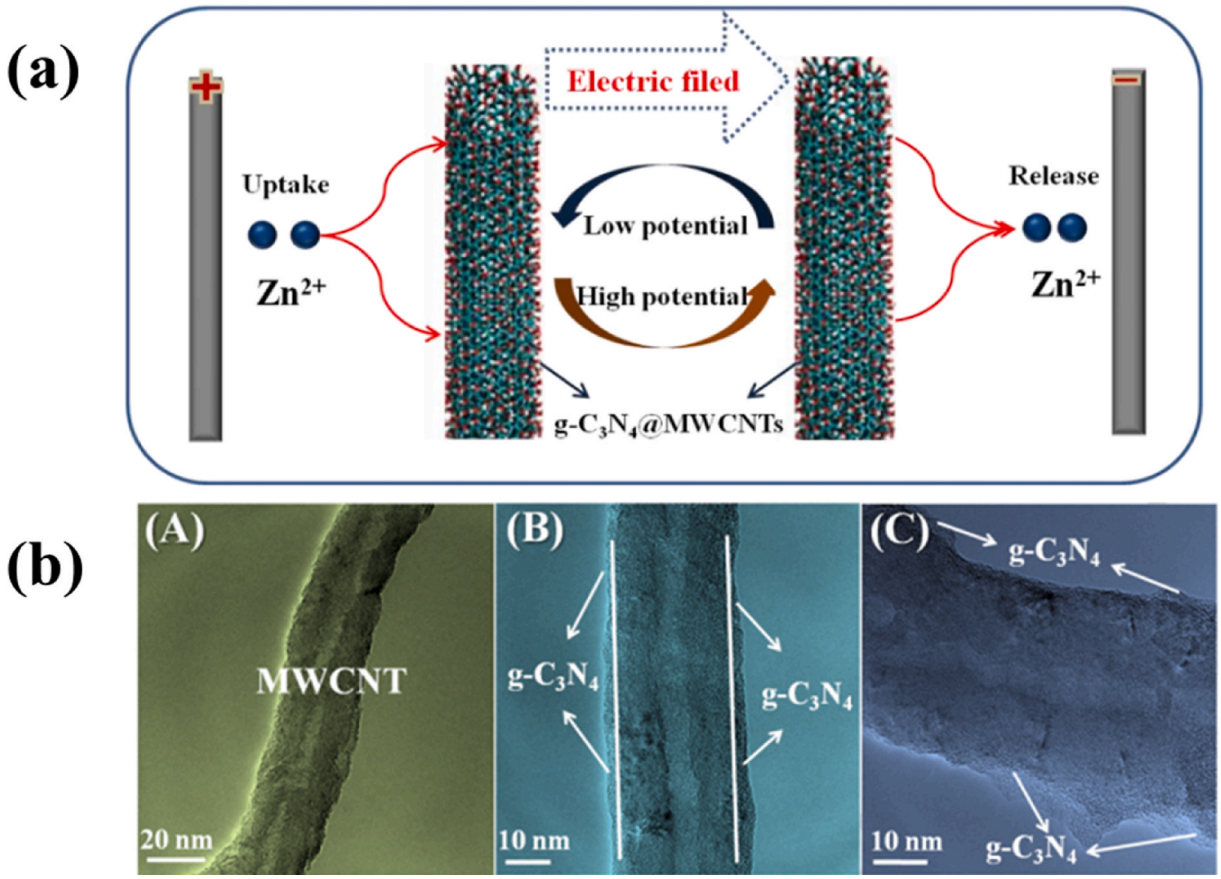

Fig. 15. Illustration of continual separation of Zn^{2+} ions across ESIP membrane (a) TEM images of MWCNTs (A) and MWCNTs (B, C) (b) [110].

hybrid mem-branes remarkable cleansing characteristics after 180 min of UV irradiation. Filtration of a combination of g-C_3N_4 and GO nanostructure on PVDF membrane provisions were used by Shi et al. to manufacture photo active membranes. When tested against different oily emulsions, the hybrid membrane exhibited improved permeability (528–862 L m^{-2} h^{-1}) and antifouling capabilities [111]. The expanded transport channels after g-C_3N_4 were intercalated onto GO layers, the water flux was improved. The addition of TiO_2 nanoparticles to g-C_3N_4/GO membranes might further enhance their antifouling and hydrophilic characteristics. TiO_2 nanoparticles were combined with GCNS by Liu et al. to produce a 0D/2D hetero-junction [53]. Vacuum-assisted self-assembly was used to intercalate the heterojunction into GO nanosheets. Increased pore size and interlayer spacing resulted in a 40-fold increase in the pure water flow by the TiO_2/GO/g-C_3N_4 membrane. The hybrid membrane achieved 99.7% FRR after 60 min of simulating solar irradiation, demonstrating its exceptional antifouling characteristics. Further, for the treatment of oily wastewater, Li et al. developed g-C_3N_4/RGO/PDA membranes employing vacuum filtration. The introduction of g-C_3N_4 into RGO/PDA membranes increased both the exclusion ratio and permeability of attached pollutants as explained in Fig. 16 (a, b) [37]. RGO/g-C_3N_4/TiO_2 nanofiber membranes were industrialized by Venkatesh et al. for the separating of motor oil, cooking oil, hydrocarbon oil and toluene from water emulsions. The permeability and rejection efficacy of hybrid membranes was excellent as compared to the pristine membrane [50].

2.5. Desalination

Exceptional possibilities for high-performing water distillation applications using reverse/forward osmosis and nanofiltration (NF) are hybrid membranes that include g-C_3N_4 nanoparticles (FO). Nanomaterials based on g-C_3N_4 have hydrophilic properties and porous structures, which make them ideal for water transportation and molecular-sieving in desalination processes. A summary of advancements in g–C_3N_4–centered hybrid membranes for desalination is shown in Table 5.

For instance, due to the easy mode of handling, high brackish rejection efficacy, and low operating stress, the NF membranes had attracted great attention in desalination [112]. By integrating g–C_3N_4–based nanomaterials, the selectivity, permeability and antifouling properties of NF membrane were improved. According to Chen et al. the introduction of GCNS to a poly amide (PA) layer on a PES substrate modified the PA layer. The flux of pure water through the tailored NF membrane was enhanced (10.5–18.8 Lm^2hbar^{-1}) and salt rejection efficiency was decreased (from 90% to 84%). The water flux decreased steadily during the long-term test for pure membrane [113]. Comparatively, PA/g-C_3N_4 membranes.

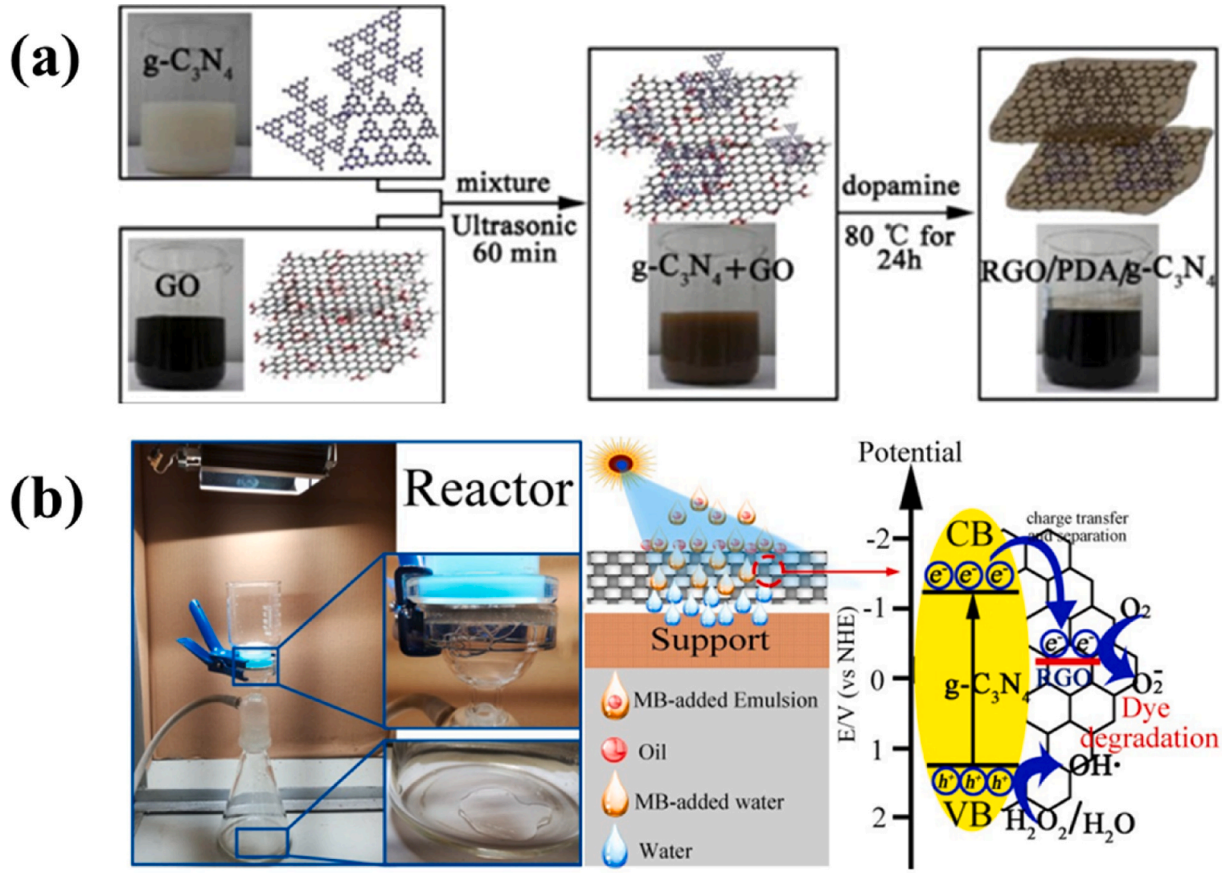

Fig. 16. Synthesis process (a) and water oil separation and photocatalytic mechanism of g-C_3N_4/RGO/PDA membranes (b) [37].

showed a significant drop in water flux initially and then stabilized, showing superior antifouling properties. NF membranes incorporating g-C_3N_4 and halloysite nanotubes (HNT) were created using vacuum clarification by Liu et al. (Fig. 17) [115]. The water flux through the g-C_3N_4/HNT NF membranes was much larger than through the HNT and g-C_3N_4 membranes. In addition, they were able to maintain their high Na_2SO_4 rejection efficiency. The HNT/g-C_3N_4 NF membranes have the following rejection order for different salts (Na_2SO_4) > ($MgSO_4$) > ($MgCl_2$) > (NaCl). Apart from the physical size sieving effect, the electrostatic interfaces among membranes and salt ions with -ve charges created by g-C_3N_4 were largely attributed to this rejection order. g-C_3N_4/HNT TFN membrane was also shown to have a steady rejection and water permeation flux over 8 h [114]. Vacuum filtration and UV irradiation were used by Li et al. to produce g-C_3N_4/RGO NF membranes. The UV irradiation period reduced the swelling effect and hydrophilicity, resulting in a significant reduction in water flux (16.4–2 Lm^2hbar^{-1}) and a significant rise in rejection efficacy (16.6–89.2%) [115]. RGO/g-C_3N_4 NF membranes desalination efficiency was influenced by Donnan exclusion and physical size sieving. The separation efficiency of the membranes made from GO/g-C_3N_4 composite was promoted via photoinduced charges. GCNS/GO/TiO-CNT NF membranes were tested for photoassisted salt rejection by Zhang et al. and the observed Na_2SO_4's retention efficiency was almost three fold with GCNS in light as compared efficiency in dark [86]. Li et al. fabricated GO/g-C_3N_4 membranes by vacuum filtration and by UV irradiation techniques and applied these membranes for desalination. The observed salt retaining sequence for the membrane with sustained water flux was (Na_2SO_4) > (NaCl) > ($MgSO_4$) > ($MgCl_2$).

As a result of RO's high salt rejection rates, it was widely used in desalination. But its poor water permeability efficiency in practical applications has been a major hurdle. Thus, RO membranes based on g-C_3N_4 were created to boost permeability without sacrificing selectivity. By integrating GCNS into the PA active sheet, Seyyed Shahabi et al. developed amended TFN-RO membranes. Improved water flow and anti-fouling performance were observed for the modified membrane [116]. GCNS functionalized (with –COOH, –SO_3H and –OH groups) was subsequently added into the PA sheet of RO membranes by Seyyed Shahabi et al. to boost its permeability. The hybrid RO membrane containing the GCNS modified with –COOH, exhibit the increased water flux (3–6.2 Lm^2hbar^{-1}) as compared to the TFN-RO membrane [46]. Moreover, the dissociation of functional groups resulted in the formation of negative charges, which improved the antifouling ability of membrane. g-C_3N_4 was acidified and integrated into the PA layer by Gao et al. Acidification of g-C_3N_4 enhanced the dispersion property, reduced the agglomeration of nanosheets and generated extra water transport channels. This resulted in a greater pure water flux ratio (79%), compared to 1.57 Lm^2hbar^{-1} for the pure membrane, without acidified g-C_3N_4 [45]. One of the biggest problems with RO desalination membranes was their poor anti-chlorine properties. Chlorine might further limit salt

Table 5
g-C_3N_4 based membranes for desalination.

Substrate	Modifier	Synthesis technique	Type of membrane	Pressure (bar)	Pure water flux (LMH bar^{-1})	Salt	Concentration (g/L)	Rejection (%)	Ref.
PES	/	Interfacial polymerization	Nanofiltration	2	~10.5	Na_2SO_4	1	90	[113]
	GCNS				~18.8			84	
	g-C_3N_4	Vacuum filtration, interfacial polymerization		4	~13			98	[114]
	HNT				16.9			~95	
	HNT/g-C_3N_4				20.5			94.5	
Cellulose ester	GO/ protonated GCNS	Vacuum filtration		1	16.4		1.42	16.6	[115]
	RGO/ protonated GCNS	UV irradiation			2			89.2	
Alumina	GO/GCNS/ TiO-CNT	Vacuum filtration, annealing		2	16		2	67	[86]
PSF	RO/GCNS	Phase inversion, interfacial polymerization	Reverse osmosis	15	3	NaCl		99.7	[116]
	RO/GCNS				3.958			~96	
	RO/COOH-GCNS				6.12			98.1	[46]
	/	Interfacial polymerization		16	1.56875			98.8	[45]
	g-C_3N_4				2.225			98.7	
	Acidified GCNS				2.8125			98.6	
	/			15	4.45			98.4	[117]
	g-C_3N_4				5.31			97.6	
	oxidized GCNS				4.89			98	
	/			15.5	1.7			98	[42]
					3.6			99.5	
	MoS_2		Forward Osmosis		27.57		1		[118]
	HNTs				5.10				[119]
	HNTs/g-C_3N_4				18.88				

rejection and water flux by destroying amide bonds. By incorporating optimized amounts of GCNS into a PA layer, the water permeation of PA-RO membranes had increased to 30% with good salt rejection ratio (99.23%). Further, the antifouling characteristics and resistance of PA-RO membranes against chlorine were significantly improved. It has been suggested that oxygen-containing groups and NH bonds can be used to separate and fend off active chlorine and pollutants, catch chlorine radicals, and react with them more actively [120]. Forward osmosis (FO) was a new technique that relied on osmotic pressure to desalinate water. Despite the fact that FO consumes less energy and exhibit excellent recovery rate, initiatives have been undertaken to reduce internal concentration polarisation (ICP) using g–C_3N_4–based materials. The phase transfer approach was used to create a unique FO-PES-MoS_2 thin film composite (TFC) membrane by blending MoS_2 nanosheets into the substrate casting solution. The innovative FO-PES-MoS_2 TFC membranes revealed significant desalination and potential features for brackish water (Fig. 18) [118]. Innovative FO membranes were designed by integrating g-C_3N_4/RGO onto the PES substrate. Water flow through the g-C_3N_4/RGO membrane enhanced to 41.4 L m^{-2} h^{-1} that was 21% higher than for unmodified membrane. The enhanced wettability and higher porosity of g-C_3N_4/RGO might be responsible for this improvement. In addition to substrate modification, the improved FO desalination performance was further aided by g-C_3N_4 modified PA layer [42]. Rezaei-Dasht Arzhandi et al. developed a new TFN membrane by combining hydrophilic halloysite nanotubes (HNTs) and g-C_3N_4 onto polysulfone-based substrate Arzhandi et al. developed TFN membranes by inserting hydrophilic halloysite nanotubes (HNT) and g-C_3N_4 nanoparticles onto polysulfone-based substrate and interfacially crosslinked polyamide layer, respectively. It was shown that the HNTs/g-C_3N_4 TFN membrane had almost two-fold increase in water flow of 18.88 L m^2 h^{-1} compared to the HNTs TFN film (5.10 L m^{-2} h^{-1}). The flux of HNTs/g-C_3N_4 TFN membrane falls only 12% over a 20-h test, but the HNTs TFN membrane showed a 24% decrease. g-C_3N_4 might increase surface hydrophilicity, reduce water transportation paths, and generate -ve charges, all of which helped to reduce ICP [119].

2.6. 6 Application of g-C_3N_4 based films

Despite its great potential for degrading organic contaminants, practically it is challenging to recover and recycle the suspended powders of g–C_3N_4–based material from wastewater. In wastewater treatment, it is possible to eliminate contaminants by loading g-C_3N_4 powders on various substrates. It has also been widely developed to immobilize g-C_3N_4 based compounds in diverse films, rather than just adding them to membranes. Photocatalytic degradation of organic contaminants, heavy metal adsorption, and microbial inactivation are only a few of the functionalities of these hybrid films covered with g–C_3N_4–based compounds. Unlike g–C_3N_4–based membranes, g–C_3N_4–based hybrid films eliminate contaminants only via photo-degradation. For practical use, g–C_3N_4–based

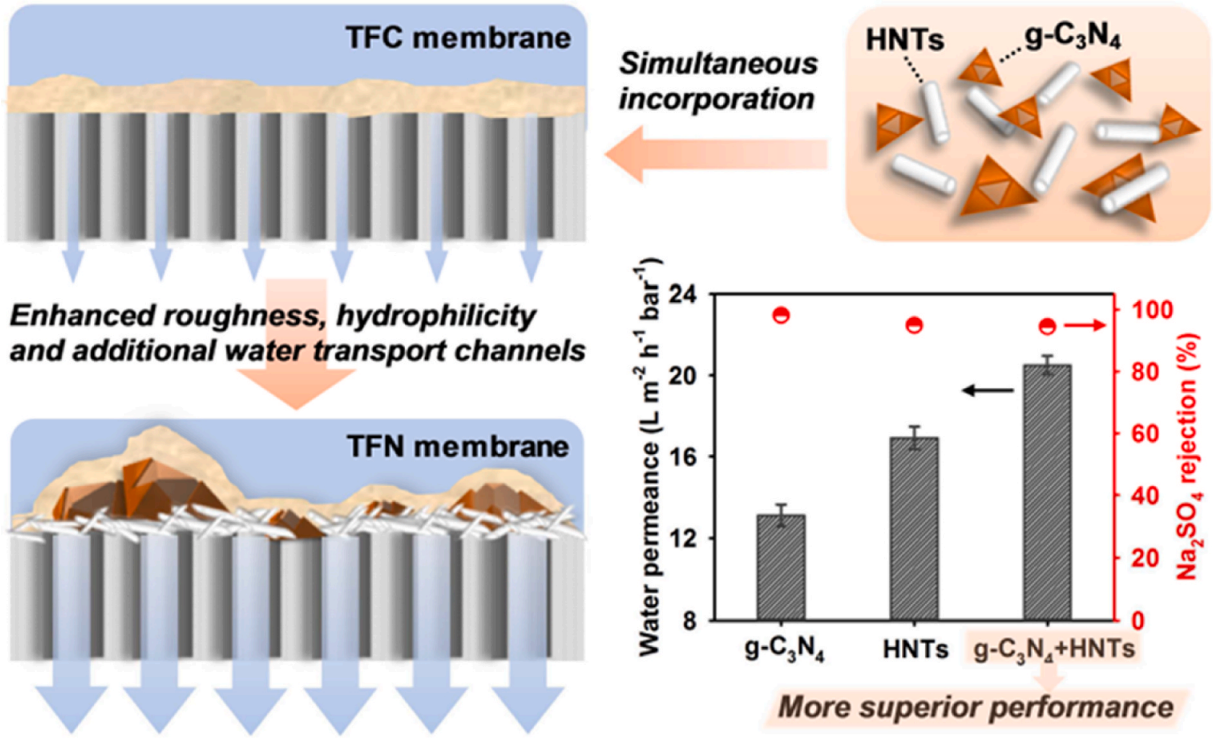

Fig. 17. Schematic diagram of synthesis of g-C_3N_4/HNT NF membranes and their efficiency [115].

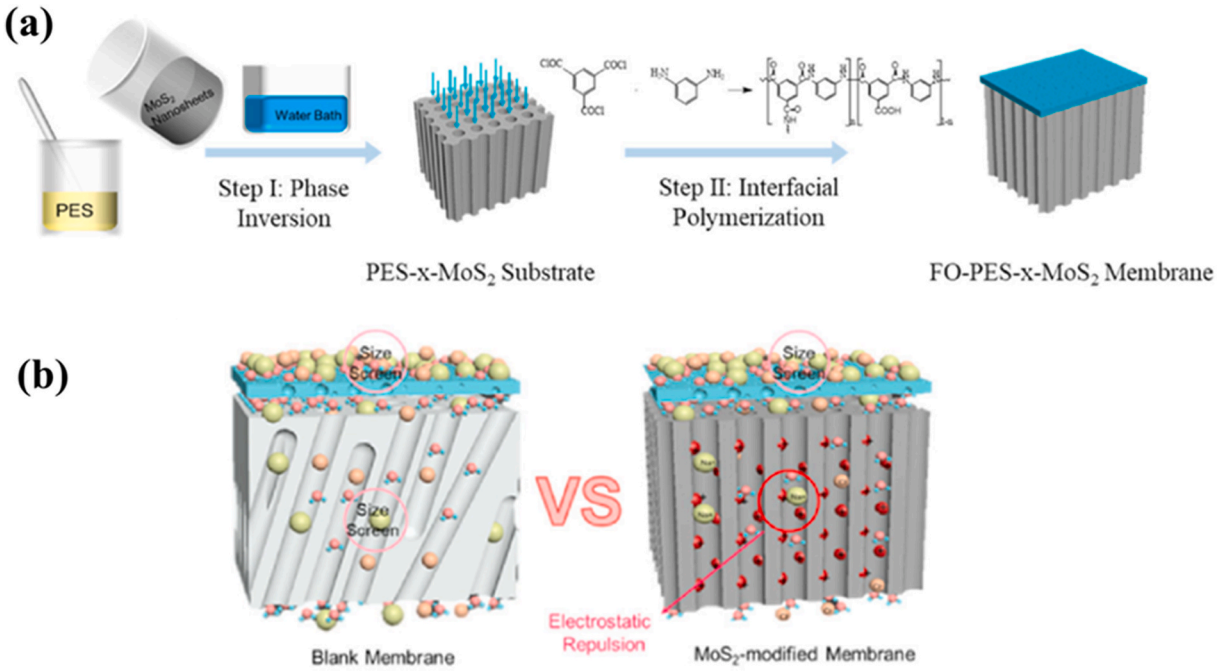

Fig. 18. Synthesis process (a) and desalination mechanism of FO-PES-x-MoS_2 membranes (b) [7].

materials are often supported by film substrates. Table 6 outlines the progress made in the production of g–C_3N_4–based hybrid films for pollutant treatment. For example, g-C_3N_4 was coated on a carbon fiber cloth by Shen et al. to create a membrane-shaped photocatalyst. Both RhB (10 mgL^{-1}) and parachlorophenol (1 mgL^{-1}) were degraded by the photocatalytic fabric under visible light irradiation.

Table 6
Removal of pollutants by g-C_3N_4 based films.

Photocatalyst	Supporting material	Reactor	Radiations	Pollutant	Concentration (mg/L)	Performance	Rate	Time (min)	Recyclability	Ref.
g-C_3N_4	PET	/	Artificial solar light	Sulfadiazine	7	Degradation	99.8%	180	99.8% after 60 h	[122]
	PMMA/CFs		Solar light	RhB	10		83%	180	75% after 20 h	[123]
	Carbon		Visible light				98%	30	/	[121]
g-C_3N_4/CdS	fiber			MB			99%	60	/	[55]
g-C_3N_4	Cu				3.2		85%	120	80% after 8 h	[127]
ZnO/g-C_3N_4/Ag	Glass						96%	60	96% after 5 h	[128]
K-g-C_3N_4		TPR	Artificial, Solar light	Phenol	980		89.06%	300	68.9% after 50 h	[129]
g-C_3N_4/RGO	Nickel foam	/	Xe lamp, $\lambda > 400$ nm	MO	5		97%	180	87.5% after 12 h	[130]
Sulfuric acid	Cellulose			RhB	10		99%	150	/	[126]
B-g-C_3N_4		TPR	Artificial solar light	Phenol	1090		81.72%	270	25.1% after 45 h	[131]
ZnAl-LDH/g-C_3N_4			Natural solar light	Phenol	830		79.35%	300	25.65% after 40 h	
g-C_3N_4/NiTi-LDH		FBR	50 W LED	MO	20		100%	240	98% after 16 h	[132]
g-C_3N_4	ITO glass	PECR	Visible light	Phenol	5		100%	300	90% after 30 h	[97]
			Bias potential: 2.5 V			TOC reduction	89.3%			
Ag/g-C_3N_4			$\lambda > 400$ nm	MB	10	degradation	72.9%	150	/	[133]
			Bias potential: 1 V							
CNTs/g-C_3N_4	PVF		Xe lamp	Tetracycline	10		98%	30	/	[134]
			Bias potential: 1.2 V							
CQD/g-C_3N_4	ITO glass		$\lambda > 420$ nm	MB	5		97.2%	180	85.4% after 15 h	[47]
			bias potential: 1 V	Phenol			51.6%	180		
CQD/g-C_3N_4/TiO2	FTO glass		85 mW cm^{-2}	1,4-Dioxane	10		77.9%	360	75% after 30 h	[135]
			$\lambda > 400$ nm bias potential: 1.2 V							
g-C_3N_4/RGO/TiO_2	PS	/	UV light	RTB	10	decolorization	99%	90	91% after 10 h	[124]
			1.07 Klux							
treated g-C_3N_4		ILAR	λ: 380–750 nm				94%	140	70% after 12 h	[136]
TiO_2/RGO/g-C_3N_4			1.97 Klux							
TiO_2/RGO/g-C_3N_4		MAR	UV light 69–72 Klux			TOC reduction	60%	140	50% after 3 h	[137]

Another carbon fiber cloth was used by Shen et al. to fabricate g-C_3N_4/CdS heterojunctions as well. Many pollutants like (e.g., 99% MB; 98% AO7; 81% tetracycline and 81% Cr^{6+}) were effectively removed by the photocatalytic cloth [55,121]. In order to create a strong 3D multilayer catalytic platform (g-C_3N_4@LMPET) for the elimination of organic contaminants, graphitic carbon nitride was implanted on the surface of the Low melting point polyester fibers (LMPET) using a hot-melt adhesive procedure. Because of its high photostability, porosity, reusability, and tensile strength, the resulting photocatalyst degraded almost all antibiotics at pH = 7 [122]. A floating g-C_3N_4/poly(methyl methacrylate)/cotton fiber film was fabricated via casting method by Wang et al. and the corresponding composite film degraded 83% RhB (10 mgL^{-1}) in 3 h and maintained its stability at an acceptable level for 20 h. Since poly(methyl methacrylate) is transparent, the film can easily absorb light and can float on water [123]. One of the most preferred substrates was carbon fiber fabric, which had a high level of strength and flexibility [117]. On the other hand, Das et al. used a polystyrene (PS) film with g-C_3N_4/RGO/TiO_2 to eliminate remazol turquoise blue from the solution (RTB) and the composite eliminated 99% of RTB (10 mgL^{-1}) within 90 min. The incorporation of g-C_3N_4 to organic polymers accelerate their decontamination and heavy metal removal efficiency [124]. For instance, Teng et al. used polyethylene bags to immobilize edge-functionalized g-C_3N_4 on them. ROS production was greatly enhanced by the presence of carboxylic and carbonyl groups on the g-C_3N_4 edge, which in turn accelerated the charge separation and microbial disinfection. Under sunlight, the modified polyethylene bags disinfected water with an initial concentration of 10^6 CFU/mL within 1 h [125]. Remarkably, the modified polyethylene bags' disinfection effectiveness remained unchanged throughout recycling. g–C_3N_4–based hybrid films may also be employed to remove heavy metals from water. Wang et al. used cellulose and sulfuric acid cured g-C_3N_4 to design photocatalytic films. Under visible light exposure the g-C_3N_4/Cellulose films successfully reduced 95% of Cr^{6+} in 1.8 h [126]. Hybrid films based on g-C_3N_4 might be supported by inorganic substrates i.e., metal film and glass etc. The Cu-g-C_3N_4 photocatalyst was formed by Sakthivel et al. using a straightforward pyrolysis technique. The Cu-g-C_3N_4 photocatalyst degraded MB more.

efficiently than Cu_2O, glass-g-C_3N_4 and Cu-g-C_3N_4 film [127]. g-C_3N_4/RGO was modified by Wang et al. by attaching to a nickel foam, and the resultant hybrid film was used to decompose MO. The reduction of photoinduced charge recombination was considerably facilitated by the heterostructure between g-C_3N_4 and RGO and consequently 97% of MO was degraded within 3 h of irradiation [130]. Under visible light, the g-C_3N_4/ZnO/Ag film on glass substrate degraded 96% of MB (3.2 mg L^{-1}) in an hour, which might be ascribed to its high smoothness and adsorption ability [128]. Recombination of photogenerated electron-hole pairs was delayed because of the electron capturing properties of Ag particles in hybrid films. Nanosheets of SnO_2/g-C_3N_4 were deposited by Faraji et al. onto the TiO_2 nanotubes and Ti plates and the resultant hybrid films were applied to eliminate the germs from the water. Under visible-light, all of the *E. coli* (1.5×10^8 CFU/mL) was killed within 2 h. But, after two runs, the antibacterial efficacy of film dropped to 94% [138].

Photocatalytic reactors (PR) were integrated with g-C_3N_4 based films and deployed to thoroughly evaluate and optimize their characteristics. A suitable PR should meet the appropriate conditions: photocatalyst-to-target contact, adequate mass transfer, and suitable light irradiation [124]. According to Das et al. a chemically fabricated recyclable RGO/TiO_2/g-C_3N_4 floating photocatalyst immobilized on a polystyrene film was tested for the decomposition of the Cu-phthalocyanine complex dye in a multiphase airlift reactor under sunlight. In immobilized form, the 60% dye was decolorization in 90 min, whereas in slurry form, under ideal circumstances, the 93% dye was decolorization in 75 min [124]. B-doped g-C_3N_4 and K-doped g-C_3N_4 were synthesized by Tripathi et al. and then integrated with zinc aluminum layered double hydroxide [129,131]. The consequent photocatalysts were attached on a glass

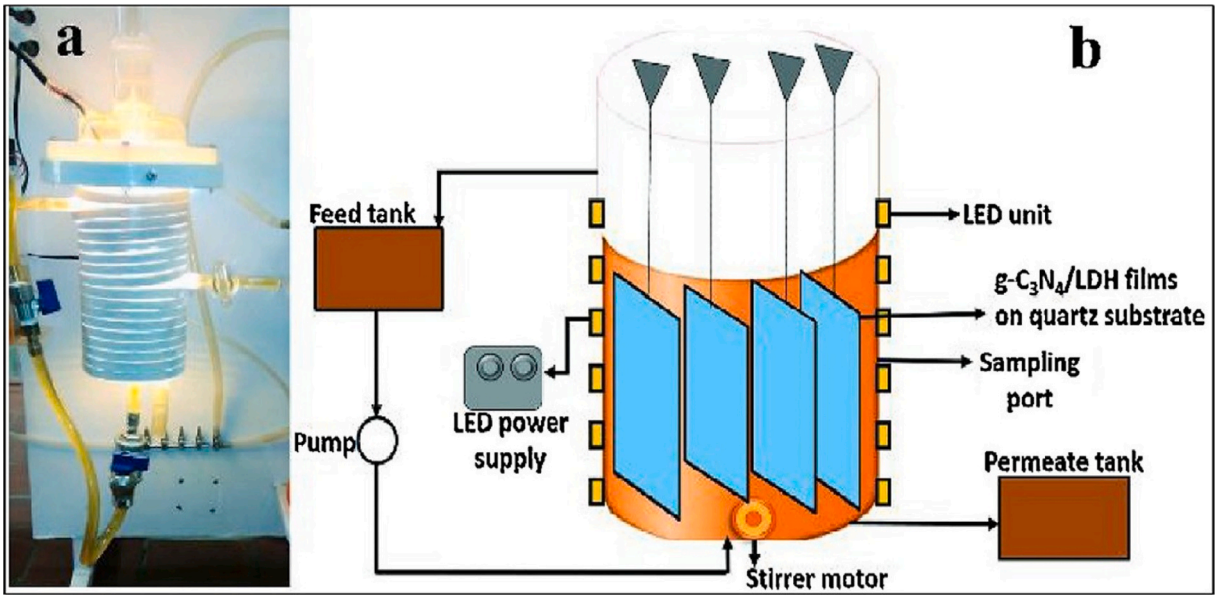

Fig. 19. The annular fix-bed reactor (a) illustration of photoreactor setup using conjugated g–C_3N_4–NiTi-LDH film-coated glass (b) [132].

plate to create a film-based tiltable plate reactor (TPR), which was subsequently used to degrade phenol from wastewater. For the removal of pollutants, layered double hydroxide (LDH) was frequently employed as catalytic support. After 300 min of treatment, the K-doped g-C_3N_4 in the TPR was able to degrade a maximum 89.06% of phenol. After 50 h of operation, the reactor was still able to decompose phenol at a rate of roughly 70% [129,131]. Similarly, Yazdani et al. described a unique fixed-bed reactor made of glass covered with NiTi-LDH film and examined its MO degradation competence as shown in Fig. 19 (a, b) [132]. With an abundance of surface defects, the NiTi-LDH is a potential contender for the modification of g-C_3N_4. The observed MO (20 mg L^{-1}) degradation efficiencies were 100% for g-C_3N_4/NiTi-LDH, 52.2% for g-C_3N_4, and 74.9% for NiTi-LDH film-coated fixed-bed reactors respectively after 240 min.

To boost the decomposition of pollutants by a synergistic photoelectric effect, photoelectrocatalytic (PEC) reactors were designed that coupled electrochemical (EC) oxidation and photocatalysis of g-C_3N_4 hybrid films. g-C_3N_4 films were used as anodes to decompose phenol under visible light radiations by Liang et al. [97]. The PEC system outperformed the EC system in photocatalytic activity against phenol (5 mg L^{-1}) and intermediates. During the PEC process, phenol was disintegrated into maleic acid and *p*-benzenediol majorly, and benzoquinone was only in trace amounts. A simple liquid-based reaction technique was used to create Ag-g-C_3N_4 films on ITO substrates. Due to the addition of Ag into g-C_3N_4, the bandgap of Ag-g-C_3N_4 was narrowed than that of g- and hence, the photocatalytic efficiency against MO dye and photocurrent density of the Ag-g-C_3N_4 film electrode were enhanced significantly [133]. Phenol-containing wastewater was treated with the help of a PEC system made of TiO_2 and g-C_3N_4/TiO_2 film electrodes. The light

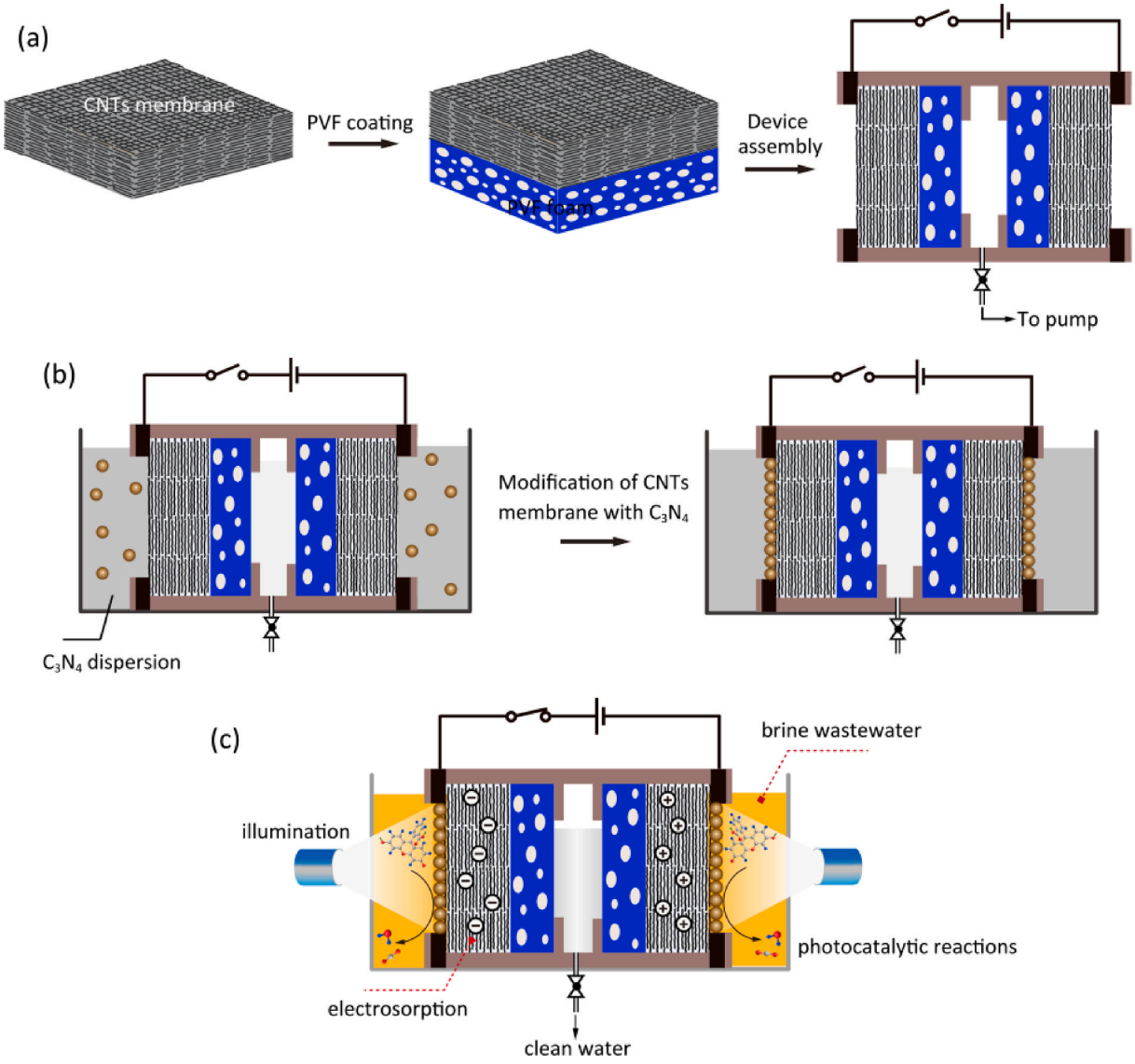

Fig. 20. Schematic drawings of the flow-through setup based on the self-assembled CNTs membrane (a) In-situ modification of the CNTs membrane with C_3N_4 nanoparticles via a simple filtration process (b) Integration of CDI and photocatalysis performances in the flow-through setup (c) [134].

irradiation accelerated the EC oxidation and allowing hydroxyl radicals to form more easily. By separating electron-hole pairs, the bias potential increased PC efficiency. Phenol was completely degraded to CO_2 and H_2O using the cutting-edge PEC technology. Hydroxyl radicals were the primary oxidative species during mineralization of phenol because of their high oxidation. Carbon quantum dots (CQDs), in addition to TiO_2, have been used as electron storage in photocatalytic systems owing to their structural parameters [139]. The degradation of MB (5 mg L^{-1}) was reached to 97.21% in 180 min using PEC effects on g-C_3N_4 nanosheets decorated with CQDs in g-C_3N_4/CQDs. CQDs may have prevented the electron-hole pairs recombination in g-C_3N_4/CQDs by trapping released electrons from g-C_3N_4. Furthermore, visible-light not only enhance the electrocatalysis but also reduced the electrode passivation [47]. Similarly, a film electrode was fabricated by Su et al. using CQD/g-C_3N_4/TiO_2 to remove 1,4-dioxane. The resultant composite was enabled to steadily eliminate the 1,4-dioxane both in near IR and visible region due to the addition of CQD [135]. A parallel-plate supercapacitor with two electrodes was also built by Ye et al. via a flow-through configuration using PVF, CNTs, and C_3N_4. The electrode in this arrangement was CNTs film moderated with g-C_3N_4 to adsorb and degrade pollutants through photocatalysis. Up to four cycles, tetracycline elimination efficacy remained at around 98%. The whole process is depicted by Fig. 20(a–c) [134].

2.7. *Recyclability of g–C_3N_4–based membranes*

Regarding practical applications, the stability and recyclability of the membrane during the waste water treatment are crucial components. Although developing such membranes that are recyclable has been always difficult. There are different studies showing the good stability and recyclability of the C_3N_4-based membrane. Qu et al., observed an initial enrichment efficiency and degradation rate of up to 96.64 and 94.30%, respectively for O-g-C3N4/GO/N-CNT membranes. They found no obvious decrease in enrichment and photocatalytic activity after three cycles under the same reaction conditions, demonstrating the high stability and outstanding reusability of these membranes [104]. Huang et al., conducted the cyclic enrichment and photodegradation tests of TCH in the presence of fabricated GO/CN@TNWs membranes under simulated solar light irradiation to realize recyclable utilization of the membrane as given by Fig. 21 [140]. Enrichment and photocatalysis activity were found to be extremely stable and to have not significantly decreased after three cycles [140]. An immersion-precipitation phase transformation was used to combine a mesoporous graphitic carbon nitride (MCN) photocatalyst with a polyvinylidene fluoride (PVDF) membrane. The membrane exhibited 97.5% degradation rate for cefixime present in real wastewater in first run under simulated sunlight. After five cycles of degradation experiment, the cefixime degradation rate remained 97.4%, indicating that MCN-PVDF membrane was stable for photocatalytic reaction. The stability of MCN-PVDF was not only due to the steady photocatalytic activity of MCN, but also attributed to the excellent mechanical and thermal stabilities of PVDF as well as its resistance to chemicals [141]. The synthesis of reduced graphene oxide/-graphitic carbon nitride sheet membrane (RGO/PDA/g-C_3N_4) was reported by Li et al. Then RGO/PDA/g-C_3N_4 composites were assembled on the surface of commercial CA (cellulose acetate) membrane to produce RGO/PDA/g–C_3N_4–CA composites membrane. The RGO/PDA/g–C_3N_4–CA composite membrane quickly degraded simultaneously soluble organic dye and separated oil/water emulsion flowing through. The composite membrane retained its steady flux and high separation efficiency even after 5 cycles under visible-light irradiation [37]. In order to make a phosphorus-doped g–C_3N_4–coated Al_2O_3 membrane, Hu et al. first immersed an Al_2O_3 substrate into a suspension of the melamine precursor. The resultant membrane exhibited excellent photocatalytic degradation and antifouling ability. Also, the dye degradation efficiency was maintained at >90% even after five regeneration cycles, demonstrating the durability of the g–C_3N_4–coated Al_2O_3 membranes [88]. In a similar vein, Shen et al. developed a well-intergrown g-C_3N_4 carbon-fiber fabric (CF/g-C_3N_4) by dipping the cloth in molten carbon disulfide and then subjecting it to thermal condensation. After being exposed to 4 cycles of RhB solution degradation, the CF/g-C_3N_4 fabric showed no discernible decline in photocatalytic activity, demonstrating excellent stability and recyclability [55]. Still, there are many citations in the literature about the stability and recyclability of the g–C_3N_4–based membranes and it is difficult for us to discuss all of them in this review. So, these studies can be discussed in some other specific review about the stability and recyclability of the g–C_3N_4–based membranes.

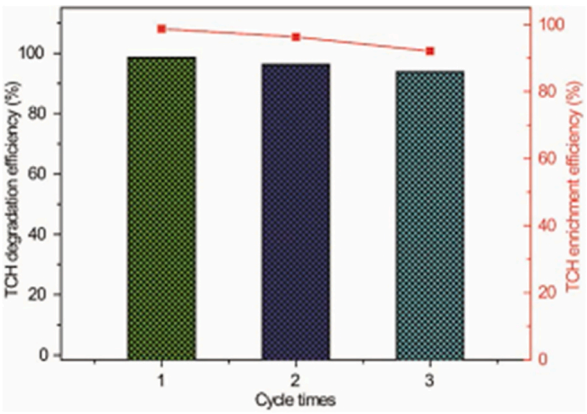

Fig. 21. Cyclic enrichment and photodegradation results of TCH in the presence of GO/CN@TNWs membrane absorbents under simulated solar light exposure [140].

2.8. Wastewater treatment mechanism

Many factors can affect the water and wastewater treatment effectiveness of g-C_3N_4 hybrid membranes. Surface roughness, hydrophilicity, surface charge, and porosity may influence the functionality of g–C_3N_4–based membranes. The introduction of g–C_3N_4–based materials might generally improve the membrane hydrophilicity [47,116]. g–C_3N_4–based hybrid membranes would thus have improved water permeability and antifouling properties. This was because the water molecules and g-C_3N_4 molecules formed hydrogen bonds, which allowed for water to diffuse more easily across the membrane and prevented contaminants from adhering to the surface [142]. The addition of g–C_3N_4–based materials, however, did not consistently alter the roughness of the membrane surface in different studies [26,42,113,128]. The roughness decreased in several instances as g–C_3N_4–based nanoparticles filled in surface voids [77]. In some cases, the development of g-C_3N_4 nanocomposite layers caused the roughness to rise. As a result, each situation's impact on the filtering performance of hybrid membranes based on g-C_3N_4 should be examined separately [113].

Both water flux and pollutant rejection rate of membrane tended to be higher if the membrane surface charge was the same as the charge of pollutant molecules in wastewater, since electrostatic adsorption hindered the water transport channels [65]. Integrating functional groups or related elements with g–C_3N_4–based materials can make the surface charge positive or negative on demand. g–C_3N_4–based hybrid membranes have more nanochannels or nanopores than pure membranes due to their laminar structure [43]. g-C_3N_4 nanopores could work as water transport channels and offer a molecular sieving function [114], improving water and wastewater treatment efficiency.

Moreover, under the influence of light, ROS may destroy organic contaminants that had stuck to the surfaces of g–C_3N_4–based hybrid membranes. The h^+ of g-C_3N_4 may accumulate in the VB of its composite photocatalysts in some heterojunctions and react with OH or H_2O to create $^{\bullet}OH$, which had a greater oxidation ability than other types of ROS [30]. The possible photodegradation mechanism of sulfamethoxazole (SMX) by mpg-C_3N_4/TiO_2 has been illustrated in Fig. 22a. According to the proposed mechanism, there is a simultaneous transport of photogenerated holes from the VB of TiO_2 to g-C_3N_4 and photogenerated electrons from the CB of g-C_3N_4 to the CB of TiO_2 in mpg-C_3N_4/TiO_2 composite. Then the generated electrons can react with absorbed surface O_2 to produce reactive oxygen species (ROS) which assists the pollutants degradation. In another study, possible photocatalytic mechanism of O-g-C_3N_4/GO/N-CNT against contaminants has been proposed via Fig. 22a [30]. According to this illustration (Fig. 22b) [104], the photoinduced electrons transported from the CB of g-C_3N_4 to N-CNT and GO in heterojunctions [104]. Then, $\bullet O_2^-$ was formed by the interaction of electrons with O_2 that had been adsorbed on the surfaces of N-CNT and GO. Since, the VB edge potential of g-C_3N_4 was more negative than the typical redox potential of OH/$^{\bullet}$OH, therefore the photogenerated holes unable to oxidize OH to $^{\bullet}$OH on the VB. So, the primary ROS in photocatalytic degradation process were $\bullet O_2^-$ and h^+, while $^{\bullet}$OH had a modest impact in catalysis. It was also shown that the degrading process wasn't always dependent on direct contact between g-C_3N_4 based materials and pollutants because the produced ROS might disperse and interact with pollutants [55]. The efficiency of water and wastewater treatment was significantly impacted by both the characteristics of the g-C_3N_4 based hybrid membrane itself and the system operation circumstances. For instance, high concentrations of target pollutants would reduce the effectiveness of their degradation because unreacted pollutants would build up on the surface of the membrane and might clog the surface-active sites [132]. The membrane's surface characteristics were closely connected to solution pH, affecting its performance. In general, the pollutant rejection rate would drop if the pH value was too low [58] due to acid etching of the g-C_3N_4 lamellar structure and hydroxyl radical production [111].

Additionally, the light source had a direct impact on the photocatalytic activity of the g-C_3N_4 based membrane system. g-C_3N_4 had a band gap of around 2.7 eV [25]. Thus, all UV light and a small portion of visible light may be effectively used by g-C_3N_4. So, with an increase in light intensity, there would be more photoinduced electron-hole pairs. For instance, the FRR of CNTO/PAA/PTFE membranes, when exposed to UV light, could reach 98% and when exposed to visible light, 93%, respectively, after 15 min [10]. An external force called a bias potential was used in PEC systems to speed up the charge transfer and separation of electron-hole pairs. g-C_3N_4 based hybrid membranes were used as photoanodes [97]. The production of $^{\bullet}$OH was facilitated by the higher dissolved oxygen content brought on by EC, which also increased the degradation efficiency [143].

3. Conclusions and perspectives

Currently, extensive research has been focused on the synthesis of g–C_3N_4–based materials and their application in diverse fields. g-C_3N_4 oriented hybrid membrane have drawn the attention of researchers for treatment of wastewater due to its excellent structure, properties and ease of fabrication. These novel membranes have shown good prospect in terms of applicability and flexibility. The use of composite membranes in water filtering not only removes contaminants, but also disinfects pathogenic microorganisms. These membranes' antifouling and self-cleaning characteristics made them more appealing for water filtration. Despite this, the g-C_3N_4 composite membranes technology faced numerous obstacles, which are still being addressed.

For g-C_3N_4 based membranes the modification procedure has a significant influence on their permeability and selectivity during wastewater treatment. Surface and matrix modification are the most common modification procedures currently available. In surface modification, the reusability of the membrane was hindered by the weak adhesion between substrate and g-C_3N_4. The anchoring strength and durability of g-C_3N_4 may be improved by using some suitable support materials like PDA. Nonetheless, new substrates and modifiers are desirable to ensure the long-term immobilization of g–C_3N_4–based compounds in hybrid membrane composition. Membrane separation is negatively impacted by the aggregation and incompatibilities of g-C_3N_4 based materials in IP method. Furthermore, the photocatalytic capacity of the g-C_3N_4 submerged in the membrane matrix is hindered due to the inadequate penetration of radiations in the membrane and due to electron transportation events being hampered to some extent by the low conductivity of the coating-membrane contact. The aggregation of g-C_3N_4 may be relieved to some extent either by surface

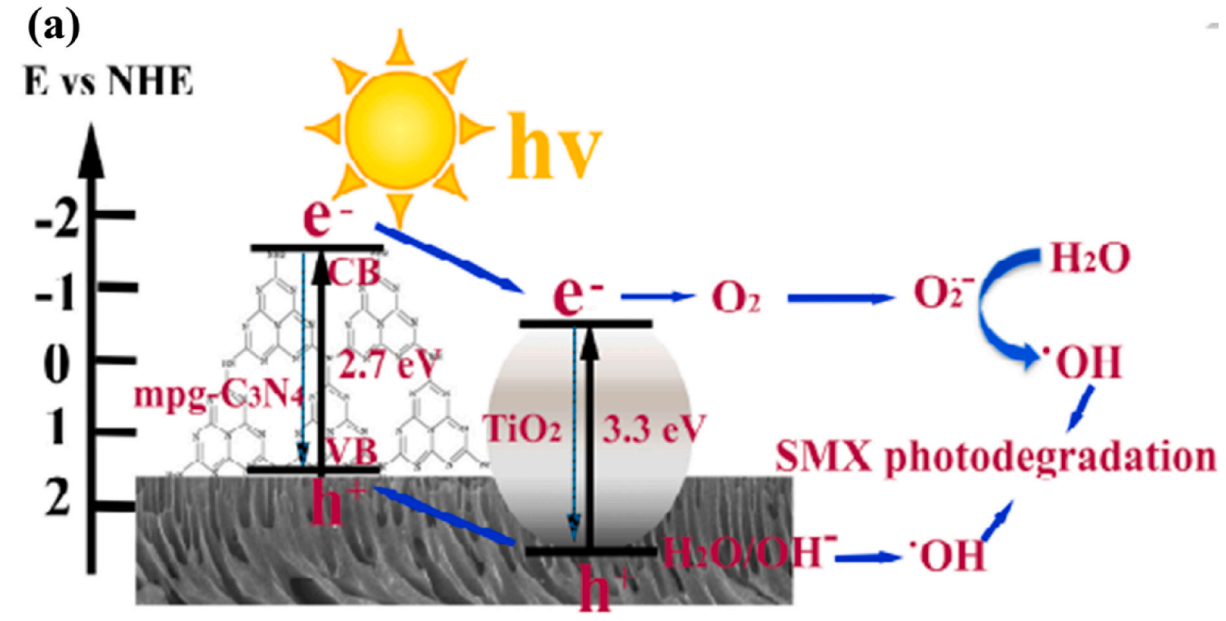

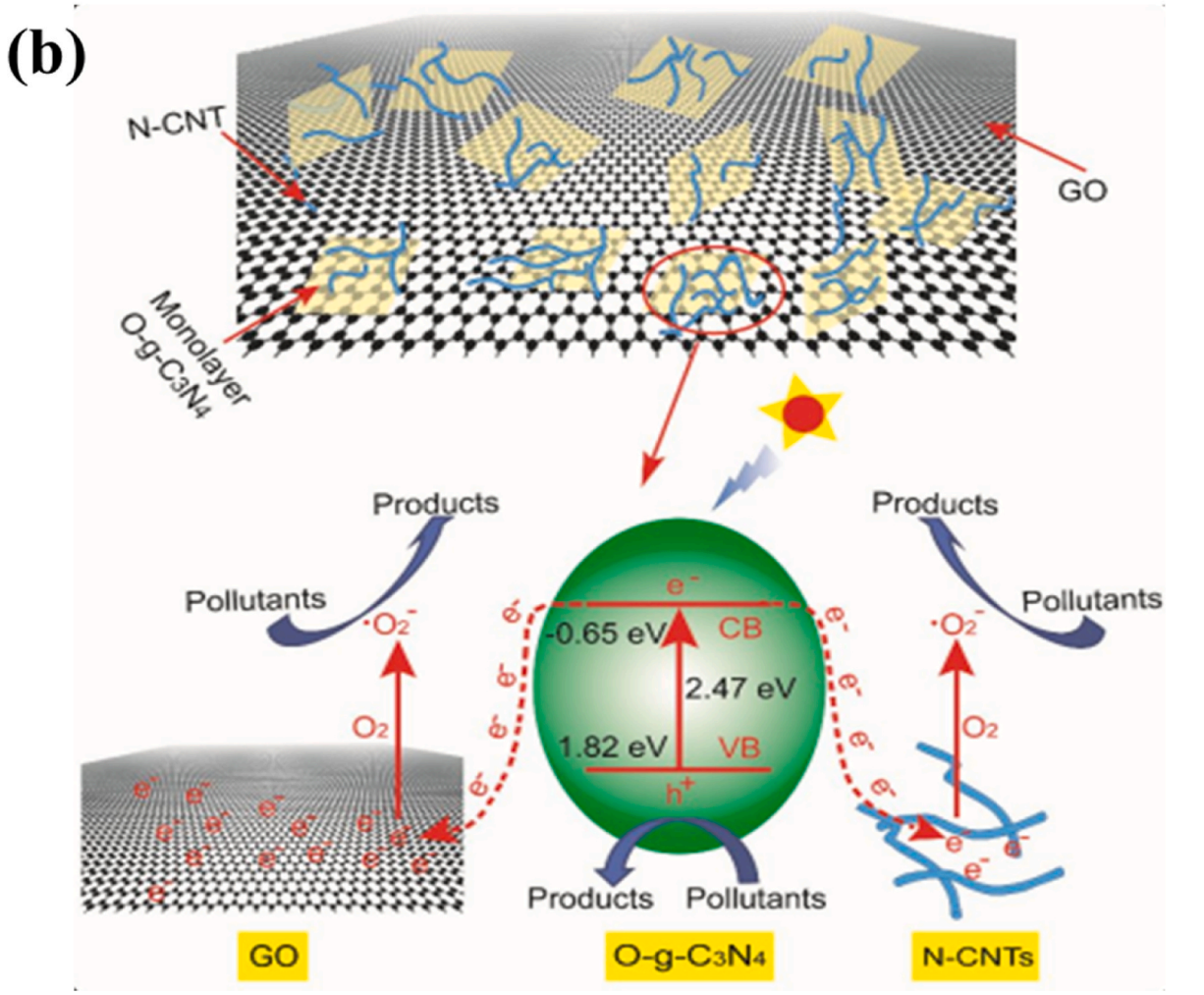

(caption on next page)

Fig. 22. Schematic design of sulfamethoxazole (SMX) photodegradation mechanism by mpg-C_3N_4/TiO_2 (a) [30]. The electron transfer mechanism and photocatalytic pollutants degradation by O–C_3N_4/GO/N-CNT under visible light illumination (b) [104].

functionalization or by the addition of interface agents. Besides, during filtration process the g-C_3N_4 based materials might be released, resulting in reduced reactive sites, lower treatment efficiency, and even contamination of the treated water. Over a short period of time, the thinnest film regions on the surface of g-C_3N_4 composite membranes become a factor of substantially decreased functionality. Conventional fabrication technologies aren't well-suited for large scale production and don't follow ecofriendly production approaches. Comparative studies on industrial point of production are rare.

Similarly, the importance of real-environment assessment is undervalued. Modeled test settings, such as self-made pollutants or bacteria, are used in the majority of investigations. These predicted settings, on the other hand, do not reflect the real-environment issues due to a lack of pollutants in feed. Most studies have used artificial wastewater as a feed solution, and the findings may not accurately reflect the efficiency of the process. Although this research concentrated on versatile applications aspects of g-C_3N_4 hybrid membranes, it is clear that their uses are still limited. In the physical realm, a feed does not just involve the pollutants described but substances like acid or alkaline can also be found in feed. When it comes to microorganisms, sea water contains far more than simple pathogenic strains. The main membrane application is to provide a large flux rate with a 100% contamination rejection rate. This membrane function requires a range of improvements, including 100% antifouling, a large surface area, regulated permeability, good mechanical resilience, passive responsiveness to feed and self-cleaning for continual and long-term operation. Any technology must be able to regenerate and reuse itself in order to be sustainable and recyclable. It's also linked to the healing of these membranes after minor damages. As a result, future study should examine how to restore and reuse these membranes.

Membranes containing pure g-C_3N_4 can utilize UV and a fraction of visible light wavelengths to destroy contaminations by the hybrid. In addition, membrane's mechanical properties may weaken under long-term exposure to UV rays. Sun light and artificial visible light, on the other hand, have a lot of prospective in terms of being environmentally benign and cost-effective. Materials such as silver, Ag_3PO_4, TiO_2 and GO, has been used to increase the photocatalytic efficiency of g-C_3N_4 based hybrid membranes by reducing the combination of electron-hole pairs. If these compounds are released from hybrid membranes, an additional study is required to examine their environmental implications. So far, majority research is focused on the degradation of pollutant, but the byproduct pollutants are overlooked. The hybrid membranes have been reported to be unable to completely decompose organic contaminants in the effluent, potentially posing a risk to the living organisms and environment.

The separation efficiency of g–C_3N_4–based membrane systems are affected by operating parameters. In membrane filtration, increase in pressure can result in a higher water flux, but it demands more mechanical strength membrane and high operational costs. Apart from the pressure, relatively large volts in g–C_3N_4–based PEC systems typically lead to better contaminant disintegration efficiencies. So, achieving a balance between the treatment effectiveness and operating costs requires optimizing the system's operating conditions.

Thus, the present article has focused the latest investigations on potential applications of g-C_3N_4 based materials to shape the next generation water purification membranes. This review has highlighted the relevant gaps in membrane effectiveness for usage as an optimal solution for actual situations, which might help protect the ecosystem from dangerous chemicals. As a result, membrane research will continue to be vital in achieving the intended goals of quality water generation and sustainability in the advanced world.

References

[1] Iqbal, et al., Bioassays based on higher plants as excellent dosimeters for ecotoxicity monitoring: a review, Chem. Int. 5 (1) (2019) 1–80.
[2] S. Noreen, et al., Chitosan, starch, polyaniline and polypyrrole biocomposite with sugarcane bagasse for the efficient removal of Acid Black dye, Int. J. Biol. Macromol. 147 (2020) 439–452.
[3] A. Kausar, et al., Development of new organic-inorganic, hybrid bionanocomposite from cellulose and clay for enhanced removal of Drimarine Yellow HF-3GL dye, Int. J. Biol. Macromol. 149 (2020) 1059–1071.
[4] S.P. Dharupaneedi, et al., Membrane-based separation of potential emerging pollutants, Separ. Purif. Technol. 210 (2019) 850–866.
[5] B.C. Hodges, E.L. Cates, J.-H. Kim, Challenges and prospects of advanced oxidation water treatment processes using catalytic nanomaterials, Nat. Nanotechnol. 13 (8) (2018) 642–650.
[6] L. Ma, et al., Fabrication and water treatment application of carbon nanotubes (CNTs)-based composite membranes: a review, Membranes 7 (1) (2017) 16.
[7] X. Li, et al., A review on graphitic carbon nitride (g-C3N4) based hybrid membranes for water and wastewater treatment, Sci. Total Environ. 792 (2021), 148462.
[8] M. Faizan, R. Ahmed, H.M. Ali, A critical review on thermophysical and electrochemical properties of Ionanofluids (nanoparticles dispersed in ionic liquids) and their applications, J. Taiwan Inst. Chem. Eng. 124 (2021) 391–423.
[9] Z. Chen, et al., Synthesis and fabrication of g-C3N4-based materials and their application in elimination of pollutants, Sci. Total Environ. 731 (2020), 139054.
[10] L. Chi, et al., Novel g-C3N4/TiO2/PAA/PTFE ultrafiltration membrane enabling enhanced antifouling and exceptional visible-light photocatalytic self-cleaning, Catal. Today 335 (2019) 527–537.
[11] X. Wang, et al., A metal-free polymeric photocatalyst for hydrogen production from water under visible light, Nat. Mater. 8 (1) (2009) 76–80.
[12] M. Javed, et al., Synergistic influences of doping techniques and well-defined heterointerface formation to improve the photocatalytic ability of the S-ZnO/GO nanocomposite, ChemistrySelect 7 (29) (2022) e202201913.
[13] M. Javed, et al., Highly Efficient Visible Light Active Cu–ZnO/Sg-C_3N_4 Nanocomposites for Efficient Photocatalytic Degradation of Organic Pollutants, 2021.
[14] Y. Liu, et al., Water desalination across multilayer graphitic carbon nitride membrane: insights from non-equilibrium molecular dynamics simulations, Carbon 140 (2018) 131–138.
[15] C. Yang, et al., CI codoped porous g-C3N4 for superior photocatalytic hydrogen evolution, Chin. J. Catal. 39 (10) (2018) 1615–1624.
[16] M. Shen, L. Zhang, J. Shi, Converting CO2 into fuels by graphitic carbon nitride-based photocatalysts, Nanotechnology 29 (41) (2018), 412001.
[17] M.A. Qamar, et al., Designing of highly active g-C3N4/Co@ ZnO ternary nanocomposites for the disinfection of pathogens and degradation of the organic pollutants from wastewater under visible light, J. Environ. Chem. Eng. 9 (4) (2021), 105534.
[18] M.A. Qamar, et al., Designing of highly active g-C3N4/Ni-ZnO photocatalyst nanocomposite for the disinfection and degradation of the organic dye under sunlight radiations, Colloids Surf. A Physicochem. Eng. Asp. 614 (2021), 126176.

[19] M. Rong, et al., Fluorescence sensing of chromium (VI) and ascorbic acid using graphitic carbon nitride nanosheets as a fluorescent "switch", Biosens. Bioelectron. 68 (2015) 210–217.
[20] S. Zhang, et al., Retraction: polymer nanodots of graphitic carbon nitride as effective fluorescent probes for the detection of Fe 3+ and Cu 2+ ions, Nanoscale 13 (36) (2021) 15481, 15481.
[21] Y. Wang, et al., Graphitic carbon nitride (gC 3 N 4)-based membranes for advanced separation, J. Mater. Chem. 8 (37) (2020) 19133–19155.
[22] L. Feng, et al., NIR-driven graphitic-phase carbon nitride nanosheets for efficient bioimaging and photodynamic therapy, J. Mater. Chem. B 4 (48) (2016) 8000–8008.
[23] Y. Ji, et al., Heptazine-based graphitic carbon nitride as an effective hydrogen purification membrane, RSC Adv. 6 (57) (2016) 52377–52383.
[24] D. Wang, et al., Next-generation multifunctional carbon–metal nanohybrids for energy and environmental applications, Environ. Sci. Technol. 53 (13) (2019) 7265–7287.
[25] S. Cao, et al., Polymeric photocatalysts based on graphitic carbon nitride, Adv. Mater. 27 (13) (2015) 2150–2176.
[26] Y. Cui, et al., Synergistic interaction of Z-scheme 2D/3D g-C3N4/BiOI heterojunction and porous PVDF membrane for greatly improving the photodegradation efficiency of tetracycline, J. Colloid Interface Sci. 586 (2021) 335–348.
[27] Y. Gong, et al., Graphitic carbon nitride polymers: promising catalysts or catalyst supports for heterogeneous oxidation and hydrogenation, Green Chem. 17 (2) (2015) 715–736.
[28] W.-J. Ong, et al., Graphitic carbon nitride (g-C3N4)-based photocatalysts for artificial photosynthesis and environmental remediation: are we a step closer to achieving sustainability? Chem. Rev. 116 (12) (2016) 7159–7329.
[29] P. Murugesan, J. Moses, C. Anandharamakrishnan, Photocatalytic disinfection efficiency of 2D structure graphitic carbon nitride-based nanocomposites: a review, J. Mater. Sci. 54 (19) (2019) 12206–12235.
[30] S. Yu, et al., Novel mpg-C3N4/TiO2 nanocomposite photocatalytic membrane reactor for sulfamethoxazole photodegradation, Chem. Eng. J. 337 (2018) 183–192.
[31] C. Jia, et al., Graphitic carbon nitride films: emerging paradigm for versatile applications, ACS Appl. Mater. Interfaces 12 (48) (2020) 53571–53591.
[32] Y. Zhang, et al., Degradation of organic pollutants by an integrated photo-Fenton-like catalysis/immersed membrane separation system, J. Hazard Mater. 244 (2013) 758–764.
[33] A. Sudhaik, et al., Review on fabrication of graphitic carbon nitride based efficient nanocomposites for photodegradation of aqueous phase organic pollutants, J. Ind. Eng. Chem. 67 (2018) 28–51.
[34] M.A. Qamar, et al., Fabrication of g-C3N4/transition metal (Fe, Co, Ni, Mn and Cr)-doped ZnO ternary composites: excellent visible light active photocatalysts for the degradation of organic pollutants from wastewater, Mater. Res. Bull. 147 (2022), 111630.
[35] C. Zhang, et al., Graphitic carbon nitride (g-C3N4)-based photocatalysts for water disinfection and microbial control: a review, Chemosphere 214 (2019) 462–479.
[36] M. Jourshabani, Z. Shariatinia, A. Badiei, Facile one-pot synthesis of cerium oxide/sulfur-doped graphitic carbon nitride (g-C3N4) as efficient nanophotocatalysts under visible light irradiation, J. Colloid Interface Sci. 507 (2017) 59–73.
[37] F. Li, et al., A Mussel-inspired method to fabricate reduced graphene oxide/g-C3N4 composites membranes for catalytic decomposition and oil-in-water emulsion separation, Chem. Eng. J. 322 (2017) 33–45.
[38] Y. Wang, et al., Water transport with ultralow friction through partially exfoliated g-C3N4 nanosheet membranes with self-supporting spacers, Angew. Chem. Int. Ed. 56 (31) (2017) 8974–8980.
[39] J. Wang, et al., Controllable construction of polymer/inorganic interface for poly (vinyl alcohol)/graphitic carbon nitride hybrid pervaporation membranes, Chem. Eng. Sci. 181 (2018) 237–250.
[40] M. Gang, et al., Graphitic carbon nitride nanosheets/sulfonated poly (ether ether ketone) nanocomposite membrane for direct methanol fuel cell application, J. Membr. Sci. 507 (2016) 1–11.
[41] X. Dong, et al., Polymers and solvents used in membrane fabrication: a review focusing on sustainable membrane development, Membranes 11 (5) (2021) 309.
[42] Y. Wang, et al., Graphene oxide modified graphitic carbon nitride as a modifier for thin film composite forward osmosis membrane, J. Membr. Sci. 475 (2015) 281–289.
[43] Y. Wang, et al., Frontispiece: water transport with ultralow friction through partially exfoliated g-C3N4 nanosheet membranes with self-supporting spacers, Angew. Chem. Int. Ed. 56 (31) (2017).
[44] R. Li, et al., Graphitic carbon nitride (g-C3N4) nanosheets functionalized composite membrane with self-cleaning and antibacterial performance, J. Hazard Mater. 365 (2019) 606–614.
[45] X. Gao, et al., Highly permeable and antifouling reverse osmosis membranes with acidified graphitic carbon nitride nanosheets as nanofillers, J. Mater. Chem. 5 (37) (2017) 19875–19883.
[46] S.S. Shahabi, et al., Novel functionalized graphitic carbon nitride incorporated thin film nanocomposite membranes for high-performance reverse osmosis desalination, Separ. Purif. Technol. 235 (2020), 116134.
[47] Q. Zhang, et al., Constructing a visible-light-driven photocatalytic membrane by g-C3N4 quantum dots and TiO2 nanotube array for enhanced water treatment, Sci. Rep. 7 (1) (2017) 1–7.
[48] N.H. Alias, et al., Photocatalytic nanofiber-coated alumina hollow fiber membranes for highly efficient oilfield produced water treatment, Chem. Eng. J. 360 (2019) 1437–1446.
[49] G.-d. Kang, Y.-m. Cao, Application and modification of poly (vinylidene fluoride)(PVDF) membranes–a review, J. Membr. Sci. 463 (2014) 145–165.
[50] K. Venkatesh, et al., Hydrophilic hierarchical carbon with TiO2 nanofiber membrane for high separation efficiency of dye and oil-water emulsion, Separ. Purif. Technol. 241 (2020), 116709.
[51] M. Soto-Herranz, et al., Effects of protonation, hydroxylamination, and hydrazination of g-C3N4 on the performance of matrimid®/g-C3N4 membranes, Nanomaterials 8 (12) (2018) 1010.
[52] Z. Tian, et al., Enhanced gas separation performance of mixed matrix membranes from graphitic carbon nitride nanosheets and polymers of intrinsic microporosity, J. Membr. Sci. 514 (2016) 15–24.
[53] Y. Liu, et al., 2D heterostructure membranes with sunlight-driven self-cleaning ability for highly efficient oil–water separation, Adv. Funct. Mater. 28 (13) (2018), 1706545.
[54] J. Song, et al., Highly flexible, core-shell heterostructured, and visible-light-driven titania-based nanofibrous membranes for antibiotic removal and E. coil inactivation, Chem. Eng. J. 379 (2020), 122269.
[55] X. Shen, et al., Growth of C3N4 nanosheets on carbon-fiber cloth as flexible and macroscale filter-membrane-shaped photocatalyst for degrading the flowing wastewater, Appl. Catal. B Environ. 219 (2017) 425–431.
[56] T. Dou, et al., Hybrid g-C3N4 nanosheet/carbon paper membranes for the photocatalytic degradation of methylene blue, Mater. Lett. 244 (2019) 151–154.
[57] X. Shen, et al., Vis-NIR light-responsive photocatalytic activity of C3N4− Ag− Ag2O heterojunction-decorated carbon-fiber cloth as efficient filter-membrane-shaped photocatalyst, ChemCatChem 11 (4) (2019) 1362–1373.
[58] Z. Wu, et al., Preparation of glycine mediated graphene oxide/g-C3N4 lamellar membranes for nanofiltration, J. Membr. Sci. 601 (2020), 117948.
[59] L. Ni, et al., Improved anti-biofouling performance of CdS/g-C3N4/rGO modified membranes based on in situ visible light photocatalysis in anammox membrane bioreactor, J. Membr. Sci. 620 (2021), 118861.
[60] R. Guo, et al., Fabrication and highly efficient dye removal characterization of beta-cyclodextrin-based composite polymer fibers by electrospinning, Nanomaterials 9 (1) (2019) 127.
[61] Y. Wang, et al., A novel Fe (OH) 3/g-C3N4 composite membrane for high efficiency water purification, J. Membr. Sci. 564 (2018) 372–381.
[62] J. Ran, et al., Endowing g-C3N4 membranes with superior permeability and stability by using acid spacers, Angew. Chem. 131 (46) (2019) 16615–16620.

[63] W. Ye, et al., High-flux nanofiltration membranes tailored by bio-inspired co-deposition of hydrophilic gC 3 N 4 nanosheets for enhanced selectivity towards organics and salts, Environmental Science: Nano 6 (10) (2019) 2958–2967.
[64] L. Liu, et al., Enhanced antipressure ability through graphene oxide membrane by intercalating g-C3N4 nanosheets for water purification, AIChE J. 65 (10) (2019), e16699.
[65] Y. Wang, et al., Enhanced water flux through graphitic carbon nitride nanosheets membrane by incorporating polyacrylic acid, AIChE J. 64 (6) (2018) 2181–2188.
[66] R. Nair, et al., Unimpeded permeation of water through helium-leak–tight graphene-based membranes, Science 335 (6067) (2012) 442–444.
[67] E.-J. Finke, et al., The risk of contracting anthrax from spore-contaminated soil–A military medical perspective, European Journal of Microbiology and Immunology 10 (2) (2020) 29–63.
[68] J. Huang, et al., Evaluation of self-cleaning and photocatalytic properties of modified g-C3N4 based PVDF membranes driven by visible light, J. Colloid Interface Sci. 541 (2019) 356–366.
[69] Z.G. Liu, et al., Efficient removal of organic dyes from water by β-cyclodextrin functionalized graphite carbon nitride composite, ChemistrySelect 2 (5) (2017) 1753–1758.
[70] B. Li, et al., Changing conventional blending photocatalytic membranes (BPMs): focus on improving photocatalytic performance of Fe3O4/g-C3N4/PVDF membranes through magnetically induced freezing casting method, Chem. Eng. J. 365 (2019) 405–414.
[71] K.-G. Zhou, et al., Self-catalytic membrane photo-reactor made of carbon nitride nanosheets, J. Mater. Chem. 4 (30) (2016) 11666–11671.
[72] W. Zhang, L. Zhou, H. Deng, Ag modified g-C3N4 composites with enhanced visible-light photocatalytic activity for diclofenac degradation, J. Mol. Catal. Chem. 423 (2016) 270–276.
[73] L.F. Dumée, et al., Towards integrated anti-microbial capabilities: novel bio-fouling resistant membranes by high velocity embedment of silver particles, J. Membr. Sci. 475 (2015) 552–561.
[74] H. Zhang, et al., Ag nanocrystals decorated g-C3N4/Nafion hybrid membranes: one-step synthesis and photocatalytic performance, Mater. Lett. 213 (2018) 218–221.
[75] H. Lan, et al., Hydrogen-bond-mediated self-assembly of carbon-nitride-based photo-Fenton-like membranes for wastewater treatment, Environ. Sci. Technol. 53 (12) (2019) 6981–6988.
[76] S. Zheng, et al., Integration of a photo-Fenton reaction and a membrane filtration using CS/PAN@ FeOOH/g-C3N4Electrospun nanofibers: synthesis, characterization, self-cleaning performance and mechanism, Appl. Catal. B Environ. 281 (2021), 119519.
[77] Y. Cui, et al., Facile preparation of antifouling g-C3N4/Ag3PO4 nanocomposite photocatalytic polyvinylidene fluoride membranes for effective removal of rhodamine B, Kor. J. Chem. Eng. 36 (2) (2019) 236–247.
[78] H. Zhao, et al., Integration of microfiltration and visible-light-driven photocatalysis on g-C3N4 nanosheet/reduced graphene oxide membrane for enhanced water treatment, Appl. Catal. B Environ. 194 (2016) 134–140.
[79] Y. Shi, et al., Stable LBL self-assembly coating porous membrane with 3D heterostructure for enhanced water treatment under visible light irradiation, Chemosphere 252 (2020), 126581.
[80] Y. Wei, Y. Zhu, Y. Jiang, Photocatalytic self-cleaning carbon nitride nanotube intercalated reduced graphene oxide membranes for enhanced water purification, Chem. Eng. J. 356 (2019) 915–925.
[81] L. Qu, et al., Gold nanoparticles and g-C3N4-intercalated graphene oxide membrane for recyclable surface enhanced Raman scattering, Adv. Funct. Mater. 27 (31) (2017), 1701714.
[82] M. Sun, et al., Fabrication of novel g-C3N4 nanocrystals decorated Ag3PO4 hybrids: enhanced charge separation and excellent visible-light driven photocatalytic activity, J. Hazard Mater. 339 (2017) 9–21.
[83] A. Brunetti, et al., CO2 reduction by C3N4-TiO2 Nafion photocatalytic membrane reactor as a promising environmental pathway to solar fuels, Appl. Catal. B Environ. 255 (2019), 117779.
[84] S. Leong, et al., TiO2 based photocatalytic membranes: a review, J. Membr. Sci. 472 (2014) 167–184.
[85] X. Wang, et al., Graphene oxide-based polymeric membranes for water treatment, Adv. Mater. Interfac. 5 (15) (2018), 1701427.
[86] Q. Zhang, et al., A multifunctional graphene-based nanofiltration membrane under photo-assistance for enhanced water treatment based on layer-by-layer sieving, Appl. Catal. B Environ. 224 (2018) 204–213.
[87] M. Kasinathan, S. Thiripuranthagan, A. Sivakumar, A facile fabrication of Br-modified g-C3N4/rGO composite catalyst for enhanced visible photocatalytic activity towards the degradation of harmful dyes, Mater. Res. Bull. 130 (2020), 110870.
[88] C. Hu, et al., Phosphorus-doped g-C3N4 integrated photocatalytic membrane reactor for wastewater treatment, J. Membr. Sci. 580 (2019) 1–11.
[89] X. Chen, et al., Functional PVDF ultrafiltration membrane for Tetrabromobisphenol-A (TBBPA) removal with high water recovery, Water Res. 181 (2020), 115952.
[90] N.E. Salim, et al., Effects of hydrophilic surface macromolecule modifier loading on PES/Og-C3N4 hybrid photocatalytic membrane for phenol removal, Appl. Surf. Sci. 465 (2019) 180–191.
[91] N.E. Salim, et al., Preparation and characterization of hydrophilic surface modifier macromolecule modified poly (ether sulfone) photocatalytic membrane for phenol removal, Chem. Eng. J. 335 (2018) 236–247.
[92] C. Chen, et al., Mn3O4 nanodots loaded g-C3N4 nanosheets for catalytic membrane degradation of organic contaminants, J. Hazard Mater. 390 (2020), 122146.
[93] Y. Wang, et al., Facile synthesis of metal free perylene imide-carbon nitride membranes for efficient photocatalytic degradation of organic pollutants in the presence of peroxymonosulfate, Appl. Catal. B Environ. 278 (2020), 118981.
[94] X. Wang, et al., Integration of membrane filtration and photoelectrocatalysis on g-C3N4/CNTs/Al2O3 membrane with visible-light response for enhanced water treatment, J. Membr. Sci. 541 (2017) 153–161.
[95] T. Arumugham, et al., Nano CuO/g-C3N4 sheets-based ultrafiltration membrane with enhanced interfacial affinity, antifouling and protein separation performances for water treatment application, J. Environ. Sci. 82 (2019) 57–69.
[96] W.-C. Lin, et al., Electrochemical photocatalytic degradation of dye solution with a TiO2-coated stainless steel electrode prepared by electrophoretic deposition, Appl. Catal. B Environ. 140 (2013) 32–41.
[97] F. Liang, Y. Zhu, Enhancement of mineralization ability for phenol via synergetic effect of photoelectrocatalysis of g-C3N4 film, Appl. Catal. B Environ. 180 (2016) 324–329.
[98] G. Wang, et al., Integration of membrane filtration and photoelectrocatalysis using a TiO2/carbon/Al2O3 membrane for enhanced water treatment, J. Hazard Mater. 299 (2015) 27–34.
[99] N.A. Khan, et al., Recent trends in disposal and treatment technologies of emerging-pollutants-A critical review, TrAC, Trends Anal. Chem. 122 (2020), 115744.
[100] J. Wang, R. Zhuan, Degradation of Antibiotics by Advanced Oxidation Processes: an Overview, vol. 701, Science of the Total Environment, 2020, 135023.
[101] S. Zhang, et al., Construction of 1D Ag-AgBr/AlOOH plasmonic photocatalyst for degradation of tetracycline hydrochloride, Front. Chem. 8 (2020) 117.
[102] D. Lv, et al., Ecofriendly electrospun membranes loaded with visible-light-responding nanoparticles for multifunctional usages: highly efficient air filtration, dye scavenging, and bactericidal activity, ACS Appl. Mater. Interfaces 11 (13) (2019) 12880–12889.
[103] X. Du, et al., Visible-light activation of persulfate by TiO2/g-C3N4 photocatalyst toward efficient degradation of micropollutants, Chem. Eng. J. 384 (2020), 123245.
[104] L. Qu, et al., Recyclable visible light-driven Og-C3N4/graphene oxide/N-carbon nanotube membrane for efficient removal of organic pollutants, ACS Appl. Mater. Interfaces 10 (49) (2018) 42427–42435.
[105] Z. Tong, et al., Three-dimensional porous aerogel constructed by g-C3N4 and graphene oxide nanosheets with excellent visible-light photocatalytic performance, ACS Appl. Mater. Interfaces 7 (46) (2015) 25693–25701.

[106] X. Chen, et al., Plasma-induced PAA-ZnO coated PVDF membrane for oily wastewater treatment: preparation, optimization, and characterization through Taguchi OA design and synchrotron-based X-ray analysis, J. Membr. Sci. 582 (2019) 70–82.
[107] X. Chen, et al., Plasma-induced poly (acrylic acid)-TiO2 coated polyvinylidene fluoride membrane for produced water treatment: synchrotron X-Ray, optimization, and insight studies, J. Clean. Prod. 227 (2019) 772–783.
[108] Q. Bi, et al., A nanofiltration membrane prepared by PDA-C3N4 for removal of divalent ions, Water Sci. Technol. 81 (2) (2020) 253–264.
[109] Y. Yang, et al., Highly efficient defluoridation using a porous MWCNT@ NiMn-LDH composites based on ion transport of EDL coupled with ligand exchange mechanism, Separ. Purif. Technol. 223 (2019) 154–161.
[110] F. Gao, et al., A novel electrical double-layer ion transport carbon-based membrane with 3D porous structure: high permselectivity for dilute zinc ion separation, Chem. Eng. J. 380 (2020), 122413.
[111] Y. Shi, et al., Evaluation of self-cleaning performance of the modified g-C3N4 and GO based PVDF membrane toward oil-in-water separation under visible-light, Chemosphere 230 (2019) 40–50.
[112] Y. Han, Z. Xu, C. Gao, Ultrathin graphene nanofiltration membrane for water purification, Adv. Funct. Mater. 23 (29) (2013) 3693–3700.
[113] J. Chen, et al., Synthesis and characterization of gC 3 N 4 nanosheet modified polyamide nanofiltration membranes with good permeation and antifouling properties, RSC Adv. 6 (113) (2016) 112148–112157.
[114] Y. Liu, et al., High-performance thin film nanocomposite membranes enabled by nanomaterials with different dimensions for nanofiltration, J. Membr. Sci. 596 (2020), 117717.
[115] Z. Li, et al., rGO/protonated g-C3N4 hybrid membranes fabricated by photocatalytic reduction for the enhanced water desalination, Desalination 443 (2018) 130–136.
[116] S.S. Shahabi, N. Azizi, V. Vatanpour, Synthesis and characterization of novel g-C3N4 modified thin film nanocomposite reverse osmosis membranes to enhance desalination performance and fouling resistance, Separ. Purif. Technol. 215 (2019) 430–440.
[117] B. Xu, et al., Graphitic carbon nitride based nanocomposites for the photocatalysis of organic contaminants under visible irradiation: progress, limitations and future directions, Sci. Total Environ. 633 (2018) 546–559.
[118] M.-N. Li, et al., Forward osmosis membranes for high-efficiency desalination with Nano-MoS2 composite substrates, Chemosphere 278 (2021), 130341.
[119] M. Rezaei-DashtArzhandi, et al., Development of novel thin film nanocomposite forward osmosis membranes containing halloysite/graphitic carbon nitride nanoparticles towards enhanced desalination performance, Desalination 447 (2018) 18–28.
[120] M. Ge, et al., Highly antifouling and chlorine resistance polyamide reverse osmosis membranes with g-C3N4 nanosheets as nanofiller, Separ. Purif. Technol. 258 (2021), 117980.
[121] X. Shen, et al., Construction of C3N4/CdS nanojunctions on carbon fiber cloth as a filter-membrane-shaped photocatalyst for degrading flowing wastewater, J. Alloys Compd. 851 (2021), 156743.
[122] X. Wang, et al., Effective elimination of antibiotics over hot-melt adhesive sheath-core polyester fiber supported graphitic carbon nitride under solar irradiation, Chem. Eng. J. 335 (2018) 82–93.
[123] S. Wang, et al., Floating and stable g-C3N4/PMMA/CFs porous film: an automatic photocatalytic reaction platform for dye water treatment under solar light, J. Porous Mater. 27 (2) (2020) 465–472.
[124] S. Das, H. Mahalingam, Exploring the synergistic interactions of TiO2, rGO, and g-C3N4 catalyst admixtures in a polystyrene nanocomposite photocatalytic film for wastewater treatment: unary, binary and ternary systems, J. Environ. Chem. Eng. 7 (4) (2019), 103246.
[125] Z. Teng, et al., Edge-functionalized g-C3N4 nanosheets as a highly efficient metal-free photocatalyst for safe drinking water, Chem 5 (3) (2019) 664–680.
[126] S. Wang, et al., Highly flexible and stable carbon nitride/cellulose acetate porous films with enhanced photocatalytic activity for contaminants removal from wastewater, J. Hazard Mater. 384 (2020), 121417.
[127] T. Sakthivel, R. Ramachandran, K. Kirubakaran, Photocatalytic properties of copper-two dimensional graphitic carbon nitride hybrid film synthesized by pyrolysis method, J. Environ. Chem. Eng. 6 (2) (2018) 2636–2642.
[128] K. Ravichandran, E. Sindhuja, Fabrication of cost effective g-C3N4+ Ag activated ZnO photocatalyst in thin film form for enhanced visible light responsive dye degradation, Mater. Chem. Phys. 221 (2019) 203–215.
[129] A. Tripathi, S. Narayanan, Potassium doped graphitic carbon nitride with extended optical absorbance for solar light driven photocatalysis, Appl. Surf. Sci. 479 (2019) 1–11.
[130] X. Wang, et al., Immobilization of 2D/2D structured g-C3N4 nanosheet/reduced graphene oxide hybrids on 3D nickel foam and its photocatalytic performance, Mater. Res. Bull. 97 (2018) 306–313.
[131] A. Tripathi, S. Narayanan, Structural modification of a 2D π-conjugated polymeric material (g-C3N4) through boron doping for extended visible light absorption, Synth. Met. 260 (2020), 116284.
[132] D. Yazdani, A.A. Zinatizadeh, M. Joshaghani, Organic–inorganic Z-scheme g-C3N4-NiTi-layered double hydroxide films for photocatalytic applications in a fixed-bed reactor, J. Ind. Eng. Chem. 63 (2018) 65–72.
[133] F. Qi, et al., Ag-Doped gC 3 N 4 film electrode: fabrication, characterization and photoelectrocatalysis property, RSC Adv. 6 (84) (2016) 81378–81385.
[134] G. Ye, et al., Efficient treatment of brine wastewater through a flow-through technology integrating desalination and photocatalysis, Water Res. 157 (2019) 134–144.
[135] Y. Su, et al., Carbon quantum dots-decorated TiO2/g-C3N4 film electrode as a photoanode with improved photoelectrocatalytic performance for 1, 4-dioxane degradation, Chemosphere 251 (2020), 126381.
[136] S. Das, H. Mahalingam, Novel immobilized ternary photocatalytic polymer film based airlift reactor for efficient degradation of complex phthalocyanine dye wastewater, J. Hazard Mater. 383 (2020), 121219.
[137] S. Das, H. Mahalingam, Dye degradation studies using immobilized pristine and waste polystyrene-TiO2/rGO/g-C3N4 nanocomposite photocatalytic film in a novel airlift reactor under solar light, J. Environ. Chem. Eng. 7 (5) (2019), 103289.
[138] M. Faraji, N. Mohaghegh, A. Abedini, Ternary composite of TiO2 nanotubes/Ti plates modified by g-C3N4 and SnO2 with enhanced photocatalytic activity for enhancing antibacterial and photocatalytic activity, J. Photochem. Photobiol. B Biol. 178 (2018) 124–132.
[139] G.S. Jamila, et al., Nitrogen doped carbon quantum dots and GO modified WO3 nanosheets combination as an effective visible photo catalyst, J. Hazard Mater. 382 (2020), 121087.
[140] Y. Huang, et al., Highly efficient removal of organic pollutants from wastewater using a recyclable graphene oxide membrane intercalated with g-C3N4@ TiO2-nanowires, J. Mol. Liq. 337 (2021), 116461.
[141] F. Yang, et al., Self-cleaning, antimicrobial, and antifouling membrane via integrating mesoporous graphitic carbon nitride into polyvinylidene fluoride, J. Membr. Sci. 606 (2020), 118146.
[142] J. Wen, et al., A review on g-C3N4-based photocatalysts, Appl. Surf. Sci. 391 (2017) 72–123.
[143] Z. Wei, et al., Photoelectrocatalytic degradation of phenol-containing wastewater by TiO2/g-C3N4 hybrid heterostructure thin film, Appl. Catal. B Environ. 201 (2017) 600–606.